Maren Evensen

An Experimental Investigation of a Quasi-Counter-Flow Air-to-Air Membrane Energy Exchanger

Master's thesis in Energy and Environment
Supervisor: Hans Martin Mathisen
June 2019

Master's thesis

NTNU
Norwegian University of Science and Technology
Faculty of Engineering
Department of Energy and Process Engineering

NTNU
Norwegian University of
Science and Technology

Maren Evensen

An Experimental Investigation of a Quasi-Counter-Flow Air-to-Air Membrane Energy Exchanger

Master's thesis in Energy and Environment
Supervisor: Hans Martin Mathisen
June 2019

Norwegian University of Science and Technology
Faculty of Engineering
Department of Energy and Process Engineering

NTNU
Norwegian University of
Science and Technology

Acknowledgement

This master's thesis was written at the Department of Energy and Process Engineering at the Norwegian University of Science and Technology in Trondheim, Norway. The master's thesis consist of 30 ECTS and was written during the spring semester of 2019.

I would like to express my sincere gratitude to my supervisor Prof. Hans Martin Mathisen for his guidance throughout the semester and for giving me the opportunity to explore such an interesting subject.

Likewise, I would like to express my gratitude towards my Co-supervisor Research Scientist Peng Liu. His insight into the subject has been very helpful, and he has answered my questions more than willingly.

I would also like to thank Håvard Rekstad and the rest of the technical staff at EPT for all the help with preparing the test rig and calibration of the measurement instruments, as well as answering any questions regarding the laboratory work.

Finally, I would like to thank my fellow student Oda Kristine Gram and her Co-supervisor Maria Justo-Alonso. Without their sensors I would not have been able to carry out the second part of my experiments.

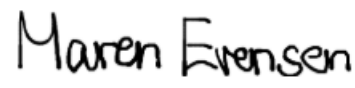

Maren Evensen, MSc. student
Trondheim, 24.06.2019

Abstract

The building sector is a significant contributor to emissions and energy use and has excellent potential to reduce this. Modern buildings have larger air tightness than traditional buildings in order to to save energy, and ventilation is the only option to provide adequate air quality. Much energy is used to heat the supply air in cold climates. As a result, heat exchangers are commonly used. However, the conventional heat exchangers do not utilise the latent heat in the air. Additionally, conventional plate heat exchangers are known to have problems with frost and condensation in the exhaust channel.

A membrane energy exchanger is proposed as a better alternative to the conventional plate heat exchanger. The membrane energy exchanger recovers both heat and moisture and is less vulnerable to frost compared to plate heat exchangers. A quasi-counter-flow configuration in MEEs has proven to obtain high effectiveness in previous studies. In this thesis, a quasi-counter-flow air-to-air membrane energy exchanger has been experimentally investigated. Both the effectiveness and the transfer of VOCs from the exhaust air to the supply air were considered. Different airflow rates, outdoor temperature, and exhaust relative humidity were tested.

The results showed that both the sensible and the latent effectiveness were quite high. Values between 88.1% and 96.1% were measured for the sensible effectiveness, and values between 87.8% and 67.2% were measured for the latent effectiveness. However, the VOC transfer through the exchanger was higher than expected. Compared to previous studies, the polypropylene membrane used in the experiments might not be the best choice.

Ideally, the MEE should achieve both a high latent effectiveness and experience a minimum of VOC transfer to the supply channel. A different membrane with high selectivity of water over other species should be investigated to accomplish this.

Sammendrag

Byggesektoren står for en stor andel av menneskers utslipp og energibruk, og det finnes et stort potensiale til å redusere dette. Moderne bygninger er mer lufttette enn tradisjonelle bygg for å spare energi, men dette kan gå på bekostning av luftkvaliteten. For å oppnå tilstrekkelig luftkvalitet gjenstår ventilasjon som den eneste løsningen. Mye av energien som blir brukt til ventilasjon går med til å varme opp luften som kommer utenfra, og varmegjenvinnere er en vanlig løsning. Tradisjonelle platevarmegjenvinnere utnytter ikke latent varme i luften, i tillegg til at de ofte har problemer med tilfrysing og konsensering på avkastsiden.

En membranbasert varmegjenvinner er foreslått som et bedre alternativ enn den tradisjonelle platevarmegjenvinneren. Membrangjenvinneren har færre problemer med tilfrysning og kondensering i avkastluften sammenlignet med vanlige varmegjenvinnere, da den kan gjenvinne både varme og fuktighet. Tidligere undersøkelser har vist at membrangjenvinnere av typen kvasi-motstrøms luft-til-luft MEE har oppnådd høy følbar og latent effektivitet. I denne oppgaven har en slik type gjenvinner blitt undersøkt eksperimentelt. Både følbar og latent effektivitiet ble undersøkt for ulike luftmengder, utetempereaturer og relativ fuktighet i avtrekksluften. I tillegg ble overføring av VOC fra avtrekksluften til tilluften i gjenvinneren undersøkt.

Resultatene viste at både følbar og latent effektivitet oppnådde høye verdier. Effektiviteten som ble målt var mellom 88.1% og 96.1% for varme, og mellom 87.8% og 67.2% for fuktighet. Derimot viste målingene av VOC at mer enn forventet ble overført fra avtrekk til tilluft. Sammenlignet med annen forskning viser det seg at en membran laget av polypropylen, slik som den som ble brukt i forsøkene, kanskje ikke er det beste alternativet.

Ideelt bør en MEE oppnå både høy latent effektivitet, og ha minimalt med overføring av VOC fra avtrekk til tilluft. Det kan tyde på at en annen type membran med høy selektivitet for vann over andre type stoffer bør testes ut for å oppnå dette.

Contents

List of Tables

List of Figures

Nomenclature

Abbreviations

AHU	Air handling unit
EATR	Exhaust air transfer rate
ERV	Energy recovery ventilator
HRV	Heat recovery ventilator
IAQ	Indoor air quality
MEE	Membrane energy exchanger
RH	Relative humidity
SFP	Specific fan power

Greek symbols

ω	Absolute humidity	kg_{water}/kg_{air}
ϕ	Relative humidity	$\%$
ρ	Air density	kg/m^3
ε	Effectiveness	

Parameters

$\dot{m}$	Mass flow rate,	kg/s
$\dot{V}$	Airflow rate	l/s

R	Ratio for heat/mass capacity	
T	Temperature	$^{\circ}C$
LMTD	Log mean temperature difference	
NTU	Number of transferring units	
P	Pressure	Nm^{-2}

Subscripts and superscripts

cou	Counter-flow
cro	Cross-flow
e	Exhaust
i	Inlet
L	Latent, moisture
o	outlet
S	Sensible, supply

Chapter 1

Introduction

The introduction states the general background and motivation for this thesis. Further, the problem description and the completed tasks are described. The work on this chapter began in the specialisation project completed by the author [1].

1.1 Background and motivation

Humans likely influence climate changes, and the new anthropogenic emissions of greenhouse gases are the highest in history. Continued emissions are expected to cause further warming and long-lasting changes in all components of the climate system. Limiting climate change would require substantial and sustained reductions in greenhouse gas emissions [2]. Globally, buildings and construction together account for 39 % of energy-related carbon dioxide emissions and 36 % of final energy use [3]. The building sector has great potential to reduce emissions and energy use further.

Furthermore, modern buildings are more airtight than old structures to improve energy efficiency, and advances in the construction sector have caused a greater use of synthetic building materials. While this provides comfortable buildings, it also facilitates higher concentrations of contaminants [4]. As a result, satisfactory ventilation of airtight, modern buildings becomes crucial.

In cold climates, much energy can be used to heat the cold supply air. Warm exhaust air contains energy which is lost when the air leaves the building, but this loss can be reduced with heat recovery.[5]. The requirements for the technical building systems have become stricter. The annual temperature efficiency should

be at least 80% in a heat recovery ventilator, and the SFP has to be maximum 1,5 $[kW/(m^3/s)]$ according to TEK17 [6].

The most common type of air-to-air heat exchangers used in Norway is the rotary heat exchanger because of its high temperature efficiency and the small risk of frosting. However, the rotary heat exchanger could experience leakage between the airflows, and this can lead to the transfer of odours and contaminants from the exhaust to the supply air streams [7]. The leakage can cause problems in apartment buildings using one central AHU to supply several living units. If odours are transferred from one living unit to others, it can leave occupants dissatisfied with the IAQ.

Instead of using rotary heat exchangers, plate heat exchangers can be used if the leakage of contaminants has to be minimised. However, there is a risk of frosting inside HRVs in cold climates, and this can cause different problems. Common problems caused by frost formation include partial or full blockage of airflow passages, increase in pressure drop or decrease in airflow rate, increase in electric power for the fans, decrease in the heat transfer rate between the two air streams and draught in the space due to low supply air temperatures [8]. The ice can occur when the warm, humid room air comes in contact with the cold surfaces of the exchanger, which is cooled by the outside air. Moisture at the exhaust air condensates in the heat exchanger and the water vapour can freeze to ice if the outside air temperature is below zero. This results in a pressure rise on the exhaust side and then a decrease in the airflow through the exhaust side [9].

Recommended relative humidity levels in office buildings and residential buildings without strict requirements are approximately 30-70% RH. This is equivalent to 5-12 g water per kg dry air at 22°C. The outdoor air contains very little moisture during the winter in cold and dry climates, and indoor humidity levels down to 10-15% RH can be registered [7]. An ERV that transfers moisture from the exhaust to the supply air stream will improve this problem.

1.2 Problem description and scope of the work

As previously mentioned, the ventilation in buildings with considerable airtightness is crucial to provide adequate IAQ. An air-to-air membrane energy exchanger is proposed as an alternative to the traditional plate heat exchanger. Both heat and moisture can be recovered by this type of exchanger, as the semi-permeable membrane allows moisture to transfer between the air streams. Previous studies have

shown that a quasi-counter-flow type MEE can achieve higher effectiveness than a cross-flow type[10].

The plate heat exchanger does not transfer any contaminants from the exhaust air stream to the supply air stream, but the transfer of exhaust air transfer rates for an MEE is unknown. The use of permeable membranes could result in the transfer of contaminants in addition to moisture. The scope of the current thesis is to complete the following tasks:

- Review state of the art research related to membranes that can be used in a membrane energy exchanger. The review should be related to the characteristics of different membranes and their performance regarding permeability and selectivity.
- Experimental investigation of the effectiveness in a quasi-counter air-to-air membrane energy exchanger. The measurements should be completed for various operating conditions.
- Evaluation of the exhaust air transfer rates of contaminants in an MEE. Sensors measuring the VOC concentrations will be installed at the test rig, and experimental measurements will be conducted to evaluate this.

Chapter 2

Membrane energy exchangers

The work on the current chapter began in the specialisation project during the fall, and then continued in this thesis [1]. Included in the chapter is an overview of the MEE and the exchanger compared to other ERVs. The leading background theory and different parameters affecting the performance are included as well.

2.1 Introduction

Configuration of the MEE

The membrane energy exchanger can be configured as both a cross flow heat exchanger or a quasi-counter-flow, as presented in figure 2.1. A quasi-counter-flow configuration consists of one rectangular counterflow area and two cross flow areas on either side of the counterflow area. A theoretical study [10] concluded that the effectiveness results in a quasi-counter-flow MEE were superior to that of a cross flow MEE.

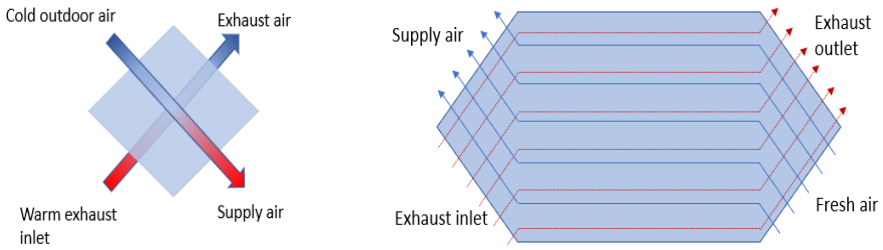

(a) Cross flow **(b)** Quasi-counter-flow

Figure 2.1: Plate type membrane exchangers

The cross flow effectiveness was in the theoretical study 10% less than that of a pure counterflow MEE [10]. To achieve the highest possible effectiveness, the cross flow areas in a quasi-counter-flow configuration should be minimised. A pure counterflow MEE, however, would be challenging to construct in practice.

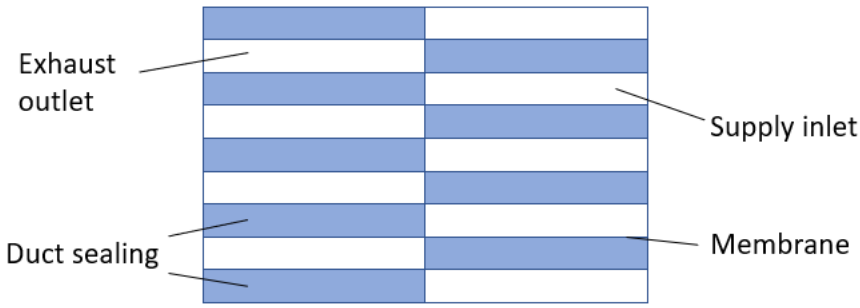

Figure 2.2: Stacked channels in a plate MEE

The plate type MEE consists of parallel layers of supply and exhaust channels separated by a flat sheet membrane, as shown in figure 2.2.

Comparison with other energy exchangers

The membrane energy exchanger mentioned above is not the only exchanger capable of recovering both heat and moisture. Two other energy exchanger types are

the energy wheel and the run-around membrane energy exchanger (RAMEE), and the working principles of the exchangers are presented in figure 2.3.

The rotary wheel exchanger consists of a porous rotating wheel driven by a motor and works as a thermal storage mass. The exhaust air and the fresh air are alternately passed through each section when the heat and moisture exchange takes place. Rotor speed is usually quite low and is ranging from 3 rpm to 15 rpm [11]. The wheel material can vary depending on the application and can be metal, fibre, ceramic, zeolite etc.[12].

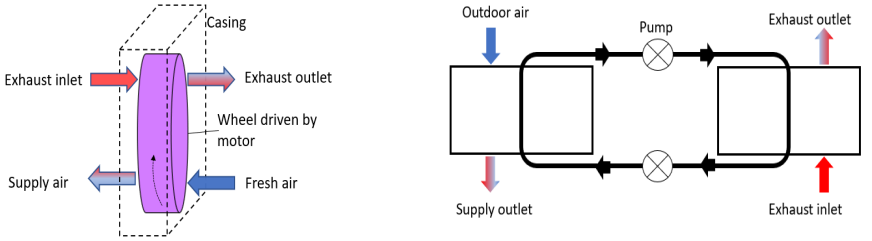

(a) Rotary wheel **(b)** The principle of a run-around heat exchanger

Figure 2.3: Other types of ERVs

The main limitation regarding the energy wheel is the significant risk of cross-contamination between the exhaust and the supply air streams. There are different leakage paths available, but the leakage will only be 0.2-1.4 % with a properly mounted rotor [7]. These exchangers are therefore a suitable choice when there are no strong odours or harmful gases in the exhaust air. Exhaust air from rooms such as kitchens or laboratories should not be used in a rotary exchanger. Rotary heat and mass exchangers are also unsuitable for hospitals and other buildings that require isolated air streams.

The Run-around membrane energy exchanger consists of two separate flat-plate liquid-to-air energy exchangers. A permeable material is separating the liquid and the air in the two exchangers in a RAMEE, allowing moisture to transfer between the air and liquid streams [11].

Each of the different exchangers contains some advantages and some drawbacks as described in table 2.1.

Table 2.1: Comparison of different air-to-air heat exchangers [13]

Type	Fixed plate	MEE	Energy Wheel	Heat Wheel	Runaround Coil
Typical ε_S [%]	50 to 80	50 to 75	50 to 85	50 to 85	55 to 65
Typical ε_L [%]	-	50 to 72	50 to 85	-	-
Advantages	No moving parts	No moving parts	Moisture or mass transfer	Compact large sizes	Exhaust airstream can be separated from supply air
	Low pressure drop Easily cleaned	Low pressure drop Low air leakage	Compact large sizes Low pressure drop Available on all ventilation platforms	Low pressure drop	Fan location not critical
Limitations	Large size at higher flow rates	Long-term maintenance and performance unknown	Supply air may require som further cooling or heating	Some EATR	Predicting performance requires accurate simulation models
		Few suppliers	Some EATR		

2.2 Heat and moisture transfer in the MEE

2.2.1 The relationship between relative humidity and moisture content

The Clapeyron-Clausius equation can be used to determine the variation of saturation pressure with temperatures. When the temperature intervals are small, the heat of vaporisation (ΔH_{vap}) can be treated as a constant[14].

$$ln\frac{P_{\mathtt{sat}}}{P_{\mathtt{ref}}} = \frac{\Delta H_{\mathtt{vap}}}{R}\left(\frac{1}{T_{\mathtt{ref}}} - \frac{1}{T}\right) \tag{2.1}$$

The saturation pressure using the Clapeyron-Clausius for a reference temperature, T_{ref} of 0°C was previously calculated and are given as[15]:

$$P_{sat} = 2.521 \cdot 10^{11} exp(-5419/T) \tag{2.2}$$

The humidity ratio is given in equation 2.3.

$$\frac{\varphi}{\omega} = \frac{P}{0.622 P_{\mathtt{sat}}} - \frac{\varphi}{0.622} \tag{2.3}$$

The second expression on the right side of the equation can usually be neglected, as it tend to have less than a 5 % effect [16]. The resulting humidity ratio when the saturation pressure is included and standard atmospheric pressure is assumed is given as:

$$\frac{\varphi}{\omega} = \frac{6.462 exp(5419/T)}{10^7} \tag{2.4}$$

2.2.2 Sensible and latent effectiveness

A method to analyse the performance of heat exchangers is to use the log mean temperature difference (LMTD). This method is easy to use when all the temperatures are known, but can be inconvenient otherwise. If only the inlet temperatures are known, use of LMTD requires an iterative procedure [17]. This can be unnecessarily cumbersome, and the well known effectiveness-NTU method is a preferable approach.

The sensible effectiveness of a heat exchanger is defined as the ratio of the actual heat transfer rate to the maximum possible heat transfer rate. For operation in heating mode, this is written as [18]:

$$\boldsymbol{\varepsilon}_S = \frac{q}{q_{max}} = \frac{C_s(t_{so} - t_{si})}{C_{min}(t_{ei} - t_{si})} \tag{2.5}$$

Where the subscripts s, e, i and o represents supply, exhaust, inlet and outlet respectively. C is the heat capacity rate:

$$C = \dot{m} c_p \tag{2.6}$$

$$NTU = \frac{UA}{C_{min}} \tag{2.7}$$

The number of transfer units (NTU) is a dimensionless parameter used for heat exchanger analysis where U is the total heat transfer coefficient, and A is the area for heat transfer used in the definition of U [18]. The NTU proves useful in relation to the effectiveness, and the correlation developed by Kays and London can be used in different problems. The first is a sizing problem where the NTU is calculated from the desired effectiveness, and then the required transfer area can be calculated. The effectiveness-NTU correlations can also be used to calculate the outlet temperatures for a given exchanger [18].

The quasi-counter flow consist of both a counterflow area and two cross-flow areas. The effectiveness-NTU correlations for the two flow configurations are relevant when considering the quasi-counter MEE. The effectiveness-NTU correlations in a cross-flow results in an infinite series, but Kays and London [18] estimated it to be:

$$\varepsilon_{cro,S/L} = 1 - exp\left[\frac{exp(-R_{1/2}NTU^{0.78}) - 1}{R_{1/2}NTU^{-0.22}}\right] \tag{2.8}$$

Zhang [19] proved that the effectiveness-NTU correlations valid for sensible heat transfer are valid for moisture transfer as well when R_1 is replaced with R_2.
R_1 represents the ratio between the heat capacity rates of the two air streams, and R_2 represents the ratio for moisture transfer.

$$R_1 = \frac{C_{min}}{C_{max}} \tag{2.9}$$

$$R_2 = \frac{\dot{m}_{min}}{\dot{m}_{max}} \tag{2.10}$$

The effectiveness of the counterflow area can be represented by NTU, as shown in equation 2.11 [17].

$$\varepsilon_{cou,S/L} = \frac{1 - e^{-NTU(1-R_{1/2})}}{1 - R_{1/2}e^{-NTU(1-R_{1/2})}} \tag{2.11}$$

When the mass flow rates are equal and $R_1 = 1$, the counterflow effectiveness can be written as:

$$\varepsilon_{cou,S/L} = \frac{NTU}{1 + NTU} \tag{2.12}$$

The effectiveness-NTU method is only one of the available methods evaluating exchanger performance. Min and Duan [20] compared the accuracy of four methods for rating the total heat exchanger performance. They concluded that even if the effectiveness-NTU method is well suited for the fast estimation of the performance, the method is not reliable for capturing various physical parameters of membrane media. This can result in inaccurate estimations of latent and total effectiveness. Out of the evaluated methods, the numerical method gave the most accurate results. The numerical method also gives a detailed distribution of different quantities of the membrane surface, which is necessary if variations in the membrane permeation properties are included. Nevertheless, the numerical method can be too time-consuming for use in most cases.

2.3 Parameters affecting the performance of the MEE

The shape of a MEE

The effectiveness of a quasi-counter-flow MEE can be affected by different parameters. One of the parameters is the exchanger shape and size. Since the MEE consist of both cross-flow and counterflow, different combinations of these could give different results regarding the effectiveness. Dvorak and Vit [21] investigated the flow and heat transfer in a quasi-counter heat exchanger of different dimensions using CFD software. The length of the exchanger was kept constant, while different heights and widths were investigated.

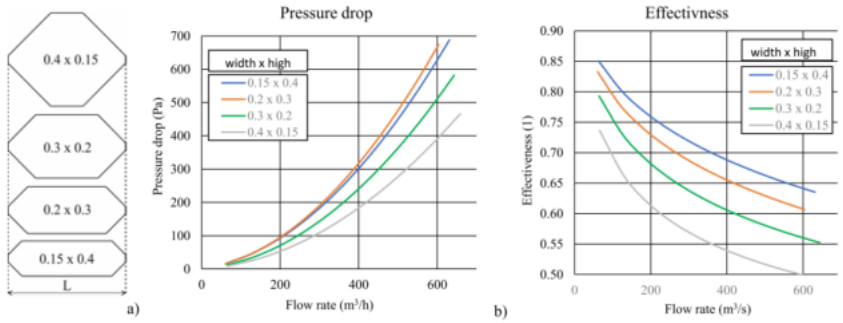

Figure 2.4: a) Pressure drop and b) effectiveness of different heat exchanger shapes with quasi-counter flow. ©Dvorak and Vit[21]

The results for different exchanger widths are shown in figure 2.4. It shows that the effectiveness is higher when the cross-flow area is minimised, which is supported by another study [10]. However, they also experienced a higher pressure drop with

the narrower exchanger surfaces, suggesting a trade-off between the effectiveness and the pressure drop when the shape of the exchanger is considered [21].

The graph also shows how the pressure drop increases for increasing airflow rate, and the effectiveness decreases for increasing airflow rate.

The channel height and membrane thickness

Amongst other factors, the performance of a membrane energy exchanger can be affected by the membrane spacing. A theoretical study investigating the effects of the spacing and thickness of membranes was conducted by Min and Su [22]. The study showed an initial increase of the total heat transfer rate as the channel height increased for a fixed fan power. Then, the heat transfer rate turned to decrease after it had attained a maximum at a specific channel height. A larger fan power leads to a more significant total heat transfer rate, with the maximum total heat transfer rate occurring at a smaller channel height.

Regarding the thickness of the membrane, both the total heat transfer rate and the enthalpy effectiveness decreased as the thickness increased. The best choice could then be a thin membrane and a moderate channel height for MEEs with a given fan [22].

Effects of outdoor operating conditions

Energy recovery ventilators are usually used in either cold and dry climates, or hot and humid climates. A theoretical study[23] showed that there is little change in sensible effectiveness at different outdoor air temperature and humidity in cold climates. The latent effectiveness, on the other hand, showed a decrease with increasing outdoor temperature but increased with increasing humidity.

In hot climates, the latent effectiveness was shown to considerably increase with increasing outdoor humidity. The sensible effectiveness showed little change with changing temperature and humidity once again. The latent effectiveness was shown to be smaller in hot weather than in cold weather, while the sensible effectiveness remained unchanged. Additionally, the membrane thermal resistance was found to be affected by the outdoor air temperature and humidity, and not only the membrane moisture resistance [23].

Chapter 3

Membranes used in MEE: A state of the art review

The current chapter focuses on the most recent publications on the subject of membranes that can be used in a MEE. Included in the subject is differences between the relevant membrane types, VOC transfer, and different support structures. This chapter is continued work from the specialisation project completed by the author [1].

3.1 Different types of membranes

Introduction

A membrane is a barrier between two phases and is usually used to separate one species from another. The most important function of a membrane is selective separation, and they are characterised by their permeability or permeance and their selectivity. Permeability is the amount of one species crossing the membrane, while selectivity is the amount of the more permeable species crossing the membrane relative to others [24]. The most common membrane material is polymers, but other materials can also be used.

Dense membranes

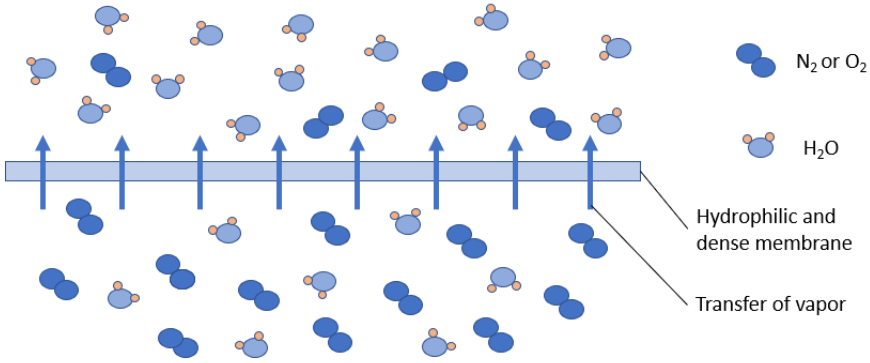

Figure 3.1: Transfer of water vapor through dense membrane. The figure is inspired by [24]

Polyvinyl pyrrolidone (PVP), polivinyl alcohol (PVA), polycrylamide (PAM), sodium alginate[Na(Alg)], chitosan (CS),cellulose acetic (CA), ethylene cellulose (EC) are examples of dense membranes [25].
Vapor permeation through dense membranes is based on the solution-diffusion mechanism. The amount of moisture permeation depends on how hydrophilic the material is. A more hydrophilic a material can adsorb more moisture. According to this theory, materials that have large quantities of hydrophilic groups such as SO_3H, -NH_2, COOH, -OH are required to have strong hydrophilicity [25].
PVA is a material with large quantities of -OH groups, and it has an excellent water vapor selectivity over several unwanted gases. Gases like CO_2 are hard to be dissolved in and permeated through it. PVA also has good membrane-forming properties, good chemical, and thermal stability, and most importantly, the material is cheap [25].

Porous membranes

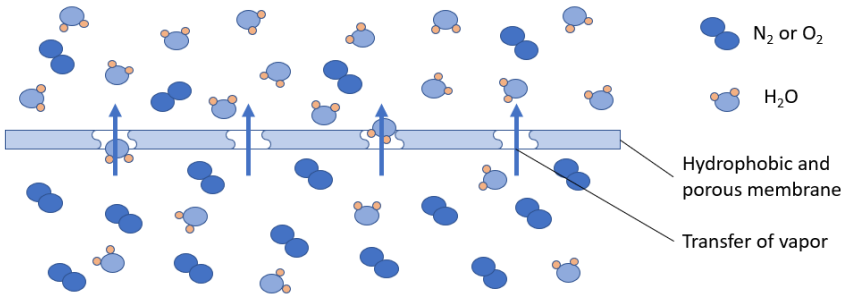

Figure 3.2: Transfer of water vapor through porous membrane.

Figure 3.2 is drawn to visualise the difference in pore size compared to a dense membrane. Porous membranes have larger pore sizes, and also a completely different transfer mechanism for moisture than dense membranes [24].

Polypropylene (PP) and polydimethylsiloxane(PDMS) are common polymer membranes characterised as porous membranes [25].

There can be different transfer mechanisms for mass transfer through a porous membrane. Poisseuille flow occurs when the pore size is large in relation to the mean free path of gas molecules, and molecule-molecule collisions between gas molecules themselves dominate. Knudsen diffusion occurs if the mean free path of the molecules is large compared to the pore size, and the molecule-wall collisions are dominant. Ordinary molecule diffusion occurs if the dominant resistance is the molecular diffusion caused by the virtually stagnant air trapped within the material pores. [26]

The Knudsen number represents the ratio of pore size to the mean free path and can decide the dominant flow. If the Knudsen number is larger than 10, the Knudsen flow is dominant. Then the Poisseuille flow can be neglected. This is the case for most microporous adsorbents used in the air conditioning industry. [26]

3.2 VOC transport in membrane exchangers

Volatile organic compounds in general

Volatile organic compounds (VOCs) are emitted as gases from certain solids or liquids, and it includes a variety of chemicals. Concentrations of many VOCs are generally higher indoors [27]. The study by Bari et al. [28] confirmed that the VOC concentrations are higher indoor than outdoor in Edmonton, Canada. More than 70% of the observed total indoor VOCs were connected to different indoor sources. Many household products include organic chemicals, and typical sources are paints, wood preservatives, cleansers, and disinfectants. These types of sources release VOCs while they are being used, but emissions can also be observed while they are stored to some degree. Except for household products, VOCs can also be found in products such as building materials and furnishings [27].

Health effects related to exposure to VOCs may include [27]:

- Eye, nose and throat irritation
- Headache, loss of coordination and nausea
- Damage to liver, kidney and central nervous system
- Some VOCs are suspected or known to cause cancer

The health effect related to different VOCs can vary greatly. Some VOCs are highly toxic, while others have no known health effect. The extent and nature of the health effects will depend on many factors, and the level of exposure and the length of time exposed are amongst these [27]. Khanchi et al. [29] examined relationships among measurements of VOCs and performed cancer and non-cancer risk assessments. Out of the studied chemicals, benzene had the highest estimated median lifetime excess cancer risk. Acetaldehyde presented the highest non-cancer risk. However, health effects related to exposure still needs more research.

Ventilation is an important measure to reduce VOC exposure, and the ventilation should be increased when using products that emit VOCs. Other steps to reduce exposure are not to open containers of unused paints and similar products indoor, and using household products according to manufacturer's directions. Generally, the supply of fresh air should be adequate when such products are in use [27].

Formaldehyde

Formaldehyde (HCHO) is one of the few indoor pollutants that can be readily measured [27], and formaldehyde can be used to evaluate the VOC transfer in heat exchangers. The gas is a colourless, flammable, and highly reactive gas at room temperature. Indoor sources of formaldehyde include combustion processes such as smoking, heating, cooking, or candle burning. Other major sources appear to be building materials and consumer products, and this especially applies to new materials and products. However, the formaldehyde emissions from new materials and products can last for several months, particularly in conditions with high relative humidity and high indoor temperatures [30]. Building materials that emit formaldehyde include furniture and wooden products such as particleboard, plywood, and medium-density fibreboard.

Formaldehyde concentrations in dwelling vary according to the age of the building, since the release of formaldehyde decreases with time; temperature and relative humidity; the air exchange rate; and the season. [30]

Concentrations above $0,2mg/m^3$ be experienced in new or renovated buildings, in new furnishings and at hot and humid times of the year. On average, the concentrations are less than $0,05mg/m^3$ in homes, and less in public buildings. The most important measures to control the concentrations of formaldehyde is the air exchange rate and the use of low-emitting materials and products.[30]

The health effects of exposure to formaldehyde in indoor air are irritation of the eyes and upper airways. Human exposure studies indicate that 0.63 mg/m3 is the threshold for trigeminal stimulation of the eyes and 0.38 mg/m3 is the threshold for subjective sensory irritation. In general, the concentration perceived by the olfactory system is lower than that triggering sensory irritation of the eyes and airways, and people may, therefore, report symptoms at levels below its sensory irritation threshold [30].

3.2.1 VOC transfer in different types of heat exchangers

Contaminants can be transferred from the exhaust air stream to the supply air stream in certain types of heat exchangers. Exhaust air transfer ratio (EATR) is defined as the tracer gas concentration difference between the supply outlet and the supply inlet divided by the concentration difference between the exhaust inlet and the supply inlet [31]. When the airflow rates on both sides are equal, EATR can be written, as shown in equation 3.1.

$$EATR = \frac{C_{i,so} - C_{i,si}}{C_{i,ei} - Ci, si} \cdot 100\% \tag{3.1}$$

The contaminant transfer mechanism can differ based on the heat exchanger type. It can be a result of air leakage between the air streams, carry-over in rotating parts of the exchanger or diffusion through a membrane wall [32]. Sometimes, the transfer of unwanted contaminants can be a result of more than one source of the transfer mechanism. A summary of possible transfer mechanisms for a few heat exchangers is presented in table 3.1.

Table 3.1: A comparison of the transfer mechanisms of contaminants for different heat exchangers [32]

Heat exchanger type	**Transfer mechanisms of contaminants**
Heat wheel	1. Air leakage between air streams 2. Carry-over from one stream to the other
Energy Wheel	1. Air leakage between air streams 2. Carry-over from one stream to the other 3. Adsorption and desorption from one air stream to the other
MEE	1. Air leakage between the air streams 2. Diffusion through the membrane wall

The amount of VOC transfer from the exhaust to the supply can differ based on the heat exchanger type. A typical VOC used as a tracer gas in experimental tests is formaldehyde, and table 3.2 gives a summary of the exhaust air transfer ratios of formaldehyde for different heat exchangers found in the literature.

Table 3.2: EATR of formaldehyde experiments found in the literature

Heat exchanger type	EATR [%]	Test type	Reference
Heat wheel	0.5-10	-	ASHRAE (2008) [13]
Energy wheel	28-29	System	Hult et al. (2014) [33]
Energy wheel	0.5-10	-	ASHRAE (2008) [13]
Fixed plate	0-5	-	ASHRAE (2008) [13]
MEE	0.3-9.6	Material	Huizing et al. (2015) [34]
MEE	0-5	-	ASHRAE (2008) [13]
RAHE	0	-	ASHRAE (2008) [13]
RAMEE	4.5-6.4	System	Patel et al. (2014) [32]

The values presented in the 2008 ASHRAE handbook [13] are noticeably smaller than the other values for the same heat exchanger type, and the values given by the handbook must be assumed as general guidelines. Values given by this handbook states the same values for the heat wheel and energy wheel, and the same goes for fixed plate HRV/ERV.

There has not been found any experimental values for the transfer of contaminants in a MEE on a system level, but only comparisons of different membranes at a material level. However, a fixed plate HRV should not have any significant transfer of contaminant, and it would be assumed that most of the transfer, if any, would go through the membrane.

3.2.2 Membrane characteristics affecting the VOC transfer

The transfer of species through a membrane can be evaluated by the use of exhaust air transfer rates (EATR), flux (J) and permeance (P/l) [34]. Equation 3.2 and equation 3.3 presents the flux and permeance, respectively.

$$J_i = \frac{\dot{V}_{so} p_{i,so} V_m}{RT \cdot A} \tag{3.2}$$

$$\frac{P_i}{l} = \frac{J_i}{p_{i,ei} - p_{i,so}} \tag{3.3}$$

Selectivity is a measure of the permeance of one chemical compound over another. In ERVs, the selectivity of water vapour over other chemical species of interest

when the indoor environment considering VOCs is evaluated.

$$\alpha_{H_2O/i} = \frac{P_{H_2O}}{P_i} \tag{3.4}$$

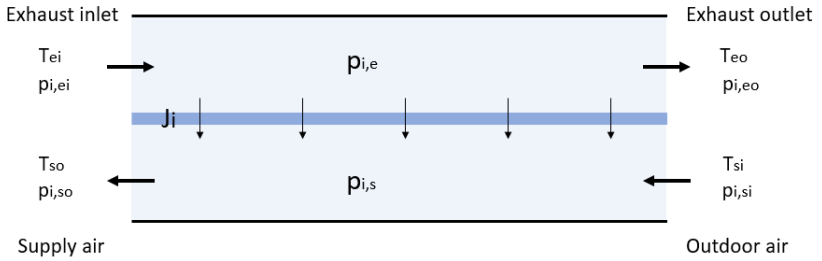

Figure 3.3: Transfer of contaminants from the exhaust stream to the supply stream. Inspired by [34]

The combination of permeance and selectivity can be a vital tool to chose materials for membranes in ERVs. Membranes with high water vapour permeance and high selectivity will be the most effective as ERV membranes as the latent effectiveness will be high, while there will be less transfer of other chemical species [35, 36, 34]. In the case of a membrane with high permeance and low selectivity, the risk of too high transfer of other chemical species, such as VOCs, is higher. These types of membranes could experience high contaminant crossover rates, and might not be very appropriate to use in ERVs. However, high moisture permeance and high selectivity of water vapour over contaminants have proved to be possible [34, 36].

The permeation rates of different polymer membranes can vary greatly depending on whether the membrane is below or above its glass transition temperature. Glassy polymers generally have an extremely low crossover ratio for contaminants. Rubbery polymer membranes, on the other hand, tend to have higher moisture permeability rates, but less selectivity. Increased moisture permeability usually leads to higher latent effectiveness. However, latent effectiveness is influenced by other factors than merely the membrane material [36].

The permeability for moisture and different VOCs, including formaldehyde, were investigated by Zhang [35] for the most commonly used membrane materials. Then, the selectivity of moisture versus VOCs was evaluated. Out of the investigated materials, PVA-1, PVP, and PAM had both high water vapour permeability

and high selectivity of water vapor relative to VOCs. PDMS had the worst score in these experiments and were followed by polypropylene.

3.3 Support spacers

Fins of different materials are commonly used in heat exchangers to work as an extended heating surface and making the exchanger more compact. There have been done extensive research on the typical plate-fin heat exchangers, and this is included in the classic textbooks such as Compact Heat Exchangers by Kays and London [18]. In a more recent study, the heat transfer in laminar plate-fin ducts was investigated, and the results suggest that the fin conductance is an important parameter including the apex angle[37].

In a MEE, support spacers are used to separate thin layers of membrane. Instead of the solid surface used in fins, the corrugated spacers have a porous mesh surface. There is very little literature on pressure drop and heat transfer with this type of spacer in heat exchangers, and there is a need for more knowledge on this topic. Only a few articles have been found with relevant corrugated spacers. Table 3.3 gives an overview of the different previously tested spacers and their properties.

Table 3.3: Spacers considered by [38] and [39]

	Spacer 1	Spacer 2	Spacer 3	Spacer 4
Supplier	-	AIL Research	Permatron	Hengrong
Material	Different	Aluminium	Aluminium	Stainless steel
Thickness (mm)	3	3	3.175	5
Corrugation pitch	8	6	9	12.5
Porosity	0.89	0.98	0.95	0.794
Filament size, d_f (mm)	0.2	0.2	0.9	0.13

J. Woods and E. Kozubal [38] investigated various support spacers for laminar airflow through membrane-bound channels, and the different geometries are shown in figure 3.4. Spacer 1 (**a**) was a triangular fin commonly used in heat exchangers. This spacer was theoretically considered as polypropylene and also materials of zero conductivity and infinite conductivity. Spacers 2 (**b**) and 3 (**c**) were considered as alternative designs with a more complex geometry, and were only experimentally measured. Different flow directions were also experimentally tested for spacer 3.

The calculated and measured f and j factors showed that spacer 3 with 90° provided the highest heat transfer, but also the highest pressure drop [38]. Spacer 2 and spacer 3 at 0° orientation gave roughly the same pressure drop as spacer 1 but provided a higher heat transfer than spacer 1 regardless of the material of spacer 1.

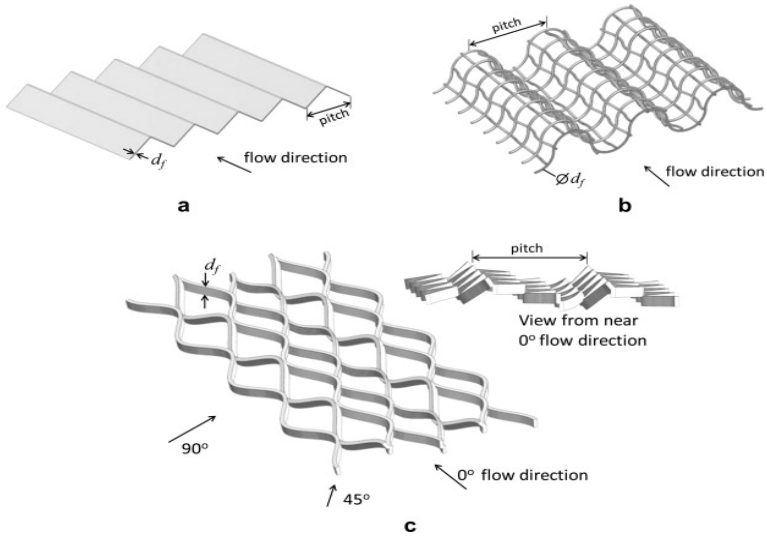

Figure 3.4: Schematics of spacers investigated by
J. Woods and E. Kozubal[38]. Reprinted with permission from Elsevier.

Mahmood et al. [39] conducted experiments related to pressure drop and heat transfer in a rectangular channel with sinusoidal porous spacers with Reynolds number ranging from 1360 to 3800, which is in the transitional flow regime. The results suggest a heat transfer enhancement for all values of transitional Reynolds number, but this is followed by a pressure penalty due to the spacer insert.

Chapter 4

Experimental Method

The experimental method chapter contains the laboratory set up, measurement equipment, the planned experiments, and uncertainty analysis.

4.1 The test rig and equipment

The test rig was previously built to experimentally investigate a MEE [40], and is redrawn in figure 4.1. The placement of the formaldehyde sensors is shown in the figure as well. The exhaust air relative humidity is regulated in the AHU. Water is supplied into the AHU, and a fan is used to blow the conditioned air through the wall in the AHU. The cold supply air is generated in an environmental chamber equipped with two CO_2 evaporators.

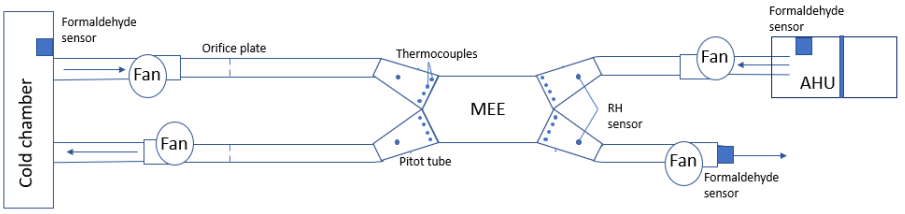

Figure 4.1: Schematics of the test rig

A picture of the real test rig is presented in figure 4.2.

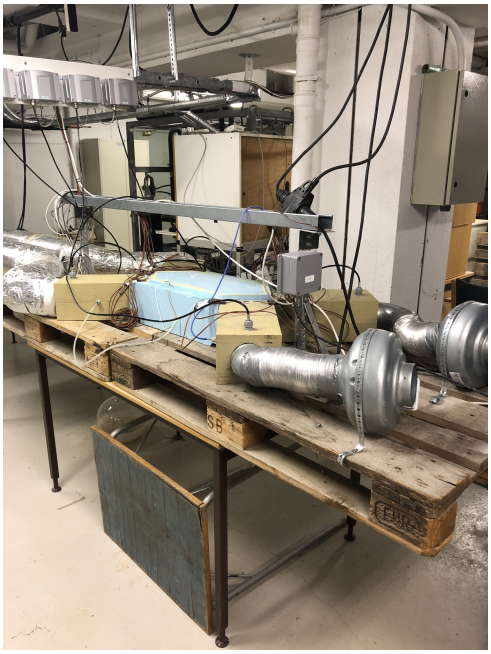

Figure 4.2: The test rig as seen in real life

Air and pressure drop measurements

Four different variable speed fans delivered balanced airflow rates, and the exhaust air is sent back to the environmental chamber to compensate for the cold supply airflow. The airflow rates were balanced by measuring the pressure difference on both sides of an orifice plate in each duct. The airflow rates were then calculated using an excel program based on the standards NS-EN ISO 5167-1 and NS-EN ISO 5167-2[41, 42].

Both the pressure drop across the MEE and the pressure difference across the orifice plate were measured using manometers and static pitot tubes. Two of the manometers were micromanometers supplied by DPM. These manometers could measure pressure between ± 0 to 7.5 kPa [43]. The most recent acquired manometer was calibrated by the manufacturer in 2018, while the other was calibrated in 2015.

Temperature measurements

The temperatures in the MEE was measured by four t-type thermocouples placed in each inlet and outlets. Thermocouples were also placed in the cold chamber,

and all the measured temperatures were displayed and logged in Labview.

Relative humidity transmitters

Relative humidity transmitters from Vaisala were calibrated and placed in each of the inlets and outlets. The RH transmitters were of the type HMT333 for ducts and tight spaces. This type of relative humidity sensor is designed for demanding industrial applications where stable measurements and extensive customisation are essential [44]. The HMT333 are typically used in cleanrooms, industrial HVAC systems, environmental chambers and processes with moderate temperature and humidity. Calibration of the RH transmitters were completed by putting each of the sensors in a salt bath for 24 hours.

Labview

Labview was used to view and log the measured temperatures and RHs. The program was also used to regulate the relative humidity in the exhaust inlet. Water supply into the exhaust inlet was regulated by choosing the time step the water would be added/shut off in the program. Figure 4.3 shows how the test rig was displayed in Labview.

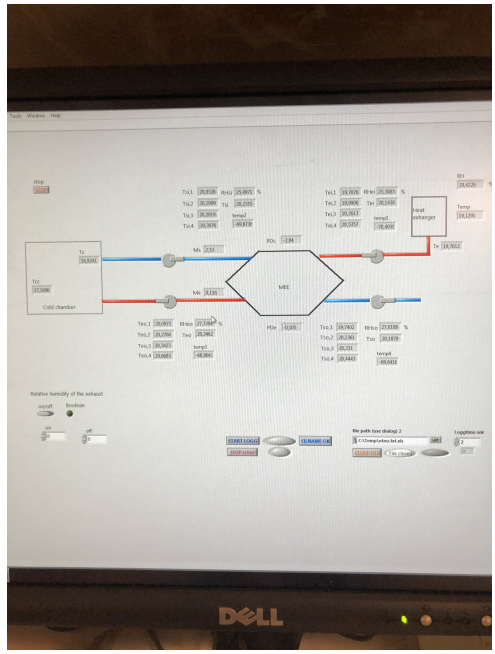

Figure 4.3: The data logging program, Labview

The exchanger core

The quasi-counter-flow MEE core consisted of plastic casing, microporous membrane, aluminium support spacers, and sealing brackets made of plastic. The MEE had previously been constructed at the EPT laboratory at NTNU, and the dimensions of the exchanger are given in table 4.1.

Table 4.1: Dimensions of the heat exchanger, previously measured [45]

Parameter	Value	unit
Exchanger width	250	mm
Length counterpart	400	mm
Number of layers	9	
Channel height	2	mm

The membrane used in the current experiments were the same as the previously used membrane. Specifications of the polypropylene membrane are presented in table 4.2.

Table 4.2: Specifications of the polypropylene membrane [40]

Properties	Value	Unit
Thermal conductivity	0.16	W/(m·K)
Membrane thickness	0.032	mm
Permeability	$1.6{\cdot}10^{-12}$	m^2/s
Density	370	kg/m^3
Porosity	41%	

To keep the membrane layers apart, support spacers had been inserted into all the channels in the MEE. Figure 4.4 displays the placements and the specifications of the spacers, which had a triangular corrugation.

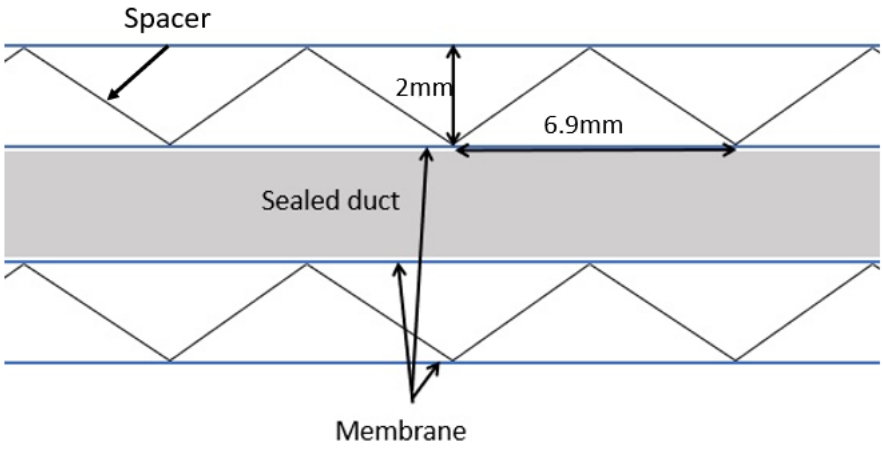

Figure 4.4: The corrugated mesh spacers

4.2 Planned effectiveness measurements

The effectiveness experiments were conducted with varying airflow rates, outdoor temperature, and exhaust inlet relative humidity. Three different values for each parameter were chosen as the main test values, and the goal was to get effectiveness measurements for all of the different combinations of these parameters. The chosen values are presented in table 4.3.

Table 4.3: The planned values for each of the regulated parameters

Parameter	Value	Unit
T_1	0	°C
T_2	-4	°C
T_3	-8	°C
V_1	4,2	l/s
V_2	6,6	l/s
V_3	8,2	l/s
φ_1	≤ 30	%
φ_2	40	%
φ_3	50	%

It was expected that it would be difficult to get exactly the planned values for each of the tests. The regulation of each of the parameters was challenging for different

reasons. For the airflow rate, it was the measured pressure difference over the orifice plate, which was slightly dependent on the temperature in the duct. However, the airflow rate was the easiest parameter to regulate. The outdoor temperature was warmer when it reached the MEE than it was in the cold chamber due to the temperature loss in the supply duct. This loss was mostly dependent on the airflow rate, but also the temperature the air had in the cold chamber. Finally, the relative humidity in the exhaust inlet was controlled by adding water to the air, and the added water amount was done by the trial and error method. Additionally, the measured relative humidity in the room before adding any water varied between 20% and 35% during the test period.

The results from the effectiveness experiments given in the next chapters are divided into results for each of the airflow rates. To make the separation and comparison easy, the experiments for each of the airflow rates were numbered from 1 to 9, as shown in table 4.4.

Table 4.4: Test indexing

	V_1			V_2			V_3		
	T_1	T_2	T_3	T_1	T_2	T_3	T_1	T_2	T_3
φ_1	1	4	7	1	4	7	1	4	7
φ_2	2	5	8	2	5	8	2	5	8
φ_3	3	6	9	3	6	9	3	6	9

4.3 Formaldehyde measurements

Formaldehyde sensors

The formaldehyde sensor is a pre-calibrated module using Dart Sensors wafer components. WZ-S formaldehyde module combines novel HCHO sensor with advanced electronic control technology, and HCHO concentration is converted directly into PPB and $\mu g/m^3$. When the HCHO arrives at working the electrode, it is oxidised instantaneously to generate an electrical signal, which is then acquired and processed by a microprocessor into the output value [46]. Table 4.5 displays the most important technical specifications for the sensor given by the manufacturer. The rest of the equipment related to the formaldehyde measurements can be found in Appendix A3.

Table 4.5: Technical specifications of the formaldehyde sensor [46]

Parameter	Condition	Value
Model		WZ-S
Detection Principle		Micro fuel cell
Detectable Gas		HCHO
Detection Range		0-2 ppm
Overload		10 ppm
Operating Temperature Range		-20°C to 50 °C
Operating Humidity Range	Non-condense	10% to 90%
Storage condition		0°C to 20 °C

Placement of the formaldehyde sensors

The formaldehyde sensors were placed in the cold chamber, by the supply outlet, and by the exhaust inlet. Figure 4.5 presents the placement of the sensors on each opening of the supply duct. The sensor in the cold chamber was connected to the wall next to the supply inlet opening, as seen in figure 4.5a. Next to the sensor and duct opening is the door connected to the laboratory room, which was closed during the experiments.

Figure 4.5b shows the supply outlet opening and the sensor connected to this opening. The sensor was connected to the fan to get as much as the supply air through the sensor rig as possible. However, since the sensor rig has a rectangular opening and the opening from the supply fan is circular, it is impossible to get all the air to go through the sensor rig.

(a) Sensor in the cold chamber

(b) Sensor connected to the supply fan

Figure 4.5: Placement of the HCHO sensors in the supply duct

Figure 4.6 presents the space where the exhaust inlet air opening is located, and the sensor was connected to the wall in this space. The duct opening for the exhaust inlet can be seen to the right in figure 4.6b. A fan and a water supply are located behind the wall in the same figure, and this is used to condition the room air during the effectiveness experiments.

(a) Sensor in the exhaust inlet

(b) The exhaust inlet room

Figure 4.6: Placement of the HCHO sensor in the exhaust inlet/room

Planned experiments

The formaldehyde experiments were conducted for three different airflow rates, and with two different supply inlet temperatures. While the chosen airflow rates were planned to be the same as the airflow rates for the effectiveness measurements, the outdoor temperatures were planned to be warmer. It was unknown how the formaldehyde sensors would react to cold temperatures, which is why warmer temperatures were chosen.

New particleboards were chosen as a formaldehyde source because new furniture and building materials are known to emit formaldehyde. The chosen particleboards belong to formaldehyde class E1 according to NS-EN 13986:2004 [47], which means that the formaldehyde emissions from the particleboards are below 0,1 ppm.

The planned experiments with the operating states for the different experiments are shown in table 4.6. Test number 0 was conducted without particleboard and is explained in detail in Appendix A5. The starting point of each of these tests was after the MEE had acquired stable conditions.

Table 4.6: The planned formaldehyde tests

Test index	$\dot{V}$ [l/s]	T_{si} [$^\circ C$]	T_{ei} [$^\circ C$]	φ_{si} [%]	φ_{ei} [%]	Particleboard state
0	6,6	15	22	30	40	Without particleboard
1	4,2	15	22	30	40	Dry
2	6,6	15	22	30	40	Dry
3	8,2	15	22	30	40	Dry
4	4,2	5	22	25	40	Dry
5	6,6	5	22	25	40	Dry
6	8,2	5	22	25	40	Dry

The formaldehyde experiments 1-6 were conducted outside of normal working hours to avoid disturbance in the measurements. During normal working hours, there were other people working in the lab with work that could emit formaldehyde, and this could lead to a large number of outside formaldehyde sources which would complicate the measurements. The formaldehyde concentrations in the room outside of the working hours were more steady.

4.4 Uncertainty

Almost all measurements include some errors and uncertainties. While it is impossible to eliminate all uncertainties, the goal should be to minimise these. There are two different types of uncertainties that are relevant to include [5]:

- Systematic errors, U_S.
- Random errors, U_T

The systematic uncertainties can be caused by both the measurement device and the operator. Some of the categories that can cause systematic errors are [48]:

1. Calibration errors
2. Data acquisition errors
3. Data reduction errors
4. Conceptual errors

Regardless of which calibration technique is chosen, there will be some systematic errors remaining. The systematic errors regarding the thermocouples were assumed to be $\pm 0,2°C$. The errors given by the supplier for the relative humidity sensors was $\pm 1\%$ due to calibration uncertainty, and with an accuracy of $\pm(1,0 + 0,008 \cdot \texttt{reading})\%$. Non-linearity, hysteresis, and repeatability were included in the accuracy [44]. The uncertainty related to the Labview readings was assumed to be negligible.

Pressure drop

The pressure drops were measured by three different manometers. Once the measurements started, it was noticed that the manometers showed different values for the same measurement, and one of the manometers showed a considerably higher value. The newest manometer was calibrated one year ago, so this was used as a reference to acquire a correlation for the manometer that showed the wrong value. This correlation is showed graphically in figure 4.7.

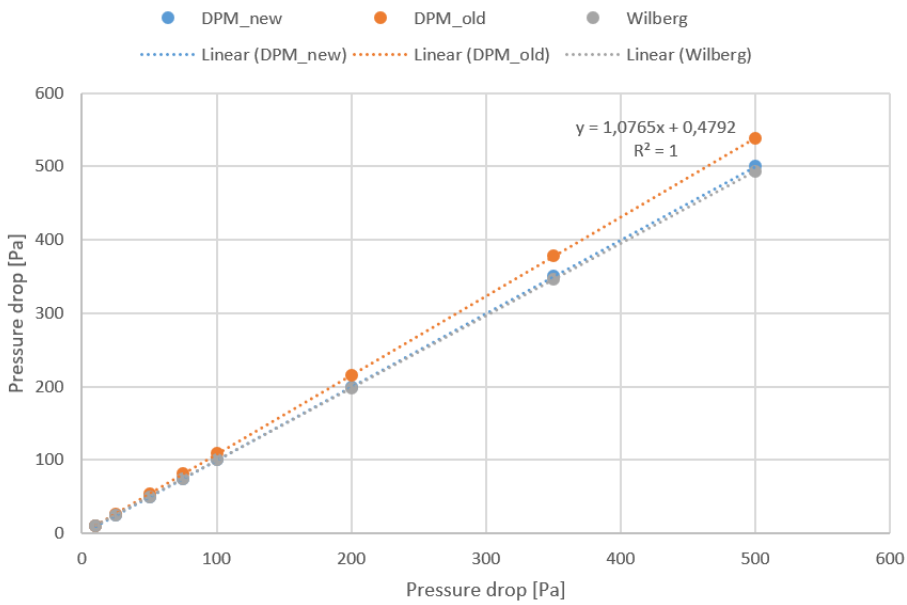

Figure 4.7: Difference in pressure drops between the manometers

The resulting correlation was then used when the old manometer was used, and this correlation had the value:

$$y = 1.0765x + 0.4792$$
$$R^2 = 1$$

Uncertainty for one simple measurement

The measured values chosen to be used in the effectiveness is the mean value of a selection of measurements in steady-state, and the formula for an average value is given in equation 4.1. The mean values are assumed to give the most accurate values and are chosen from $n = 30$ readings. The time step chosen in Labview^{TM}was 60, which was approximately two minutes.

$$\overline{x} = \frac{\Sigma x}{n} \tag{4.1}$$

To obtain the random uncertainty for one simple point, the standard deviation is used as shown in equations 4.2 and 4.3. U represents the random uncertainty and s is the standard deviation for a given parameter x with n readings.

$$s = \sqrt{\frac{\Sigma(x - \overline{x})^2}{n - 1}} \tag{4.2}$$

$$U_R = \pm \frac{s}{\sqrt{n}} \tag{4.3}$$

The total uncertainty is given by equation 4.4 as the root-sum-square (RSS) combination of the random and the systematic uncertainty.

$$U = \pm \sqrt{U_R^2 + U_S^2} \tag{4.4}$$

Uncertainty including data reduction

The general expression for the uncertainty is given in equation 4.5 [48]:

$$U = \pm \sqrt{\left(\frac{\partial f}{\partial u_1} \cdot \Delta u_1\right)^2 + ... + \left(\frac{\partial f}{\partial u_n} \cdot \Delta u_n\right)^2} \tag{4.5}$$

The data reduction equation for the moisture content i. the air is given by equation 4.6 as previously mentioned in chapter 2.

$$\omega = \frac{\varphi \cdot 10^7}{6.462 exp(\frac{5419}{T})} \tag{4.6}$$

The uncertainty for the moisture content is the given in equation 4.7.

$$U_\omega = \pm \left[\left(\frac{10^7}{6.462 exp(\frac{5419}{T})} \cdot \Delta\varphi \right)^2 \right. \tag{4.7}$$

$$\left. + \left(\frac{10^7 \cdot \varphi \frac{5419}{T^2}}{6.462 exp(\frac{5419}{T})} \cdot \Delta T \right)^2 \right]^{1/2} \tag{4.8}$$

Assuming the airflow rates are balanced, the expressions for the sensible and latent effectiveness are given in equations 4.9 and 4.10.

$$\varepsilon_S = \frac{T_{so} - T_{si}}{T_{ei} - T_{si}} \tag{4.9}$$

$$\varepsilon_L = \frac{\omega_{so} - \omega_{si}}{\omega_{ei} - \omega_{eo}} \tag{4.10}$$

The resulting total uncertainty for the sensible effectiveness and the latent effectiveness are given in equations 4.11 and 4.13, respectively. ΔT and $\Delta\omega$ in the expressions represents the total uncertainties for the temperature and the moisture.

$$U_{\varepsilon_S} = \pm \Bigg[\left(\frac{T_{so} - T_{ei}}{(T_{ei} - T_{si})^2} \cdot \Delta T_{si} \right)^2 + \left(\frac{1}{T_{ei} - T_{si}} \cdot \Delta T_{so} \right)^2 \tag{4.11}$$

$$+ \left(\frac{T_{si} - T_{so}}{(T_{ei} - T_{si})^2} \cdot \Delta T_{ei} \right)^2 \Bigg]^{1/2} \tag{4.12}$$

$$U_{\varepsilon_L} = \pm \Bigg[\left(\frac{\omega_{so} - \omega_{ei}}{(\omega_{ei} - \omega_{si})^2} \cdot \Delta \omega_{si} \right)^2 + \left(\frac{1}{\omega_{ei} - \omega_{si}} \cdot \Delta \omega_{so} \right)^2 \tag{4.13}$$

$$+ \left(\frac{\omega_{si} - \omega_{so}}{(\omega_{ei} - \omega_{si})^2} \cdot \Delta \omega_{ei} \right)^2 \Bigg]^{1/2} \tag{4.14}$$

Overview of the uncertainties

Table 4.7 provides an overview of the calculated uncertainties for measurement number 4 at airflow rate $\dot{V}_2$.

Table 4.7: The calculated uncertainties for one of the measurements

Parameter	Uncertainty for $\dot{V}_2$, test 4
T_{SI} [°C]	±0.24@-4.22
T_{SO} [°C]	±0.20@20.8
T_{EI} [°C]	±0.21@22.2
T_{EO} [°C]	±0.23@0.93
φ_{SI} [%]	±1.44@16.4
φ_{SO} [%]	±1.42@21.2
φ_{EI} [%]	±1.42@24.0
φ_{EO} [%]	±1.43@32.1
ω_{SI} [kg/kg]	±0.00004@0.0005
ω_{SO} [kg/kg]	±0.00023@0.0033
ω_{EI} [kg/kg]	±0.00025@0.0041
$\dot{V}$	±3.7%@6.8 l/s
ε_S [%]	±1.1@94.8
ε_L [%]	±8.2@78.6

Chapter 5

Results

5.1 Effectiveness measurements

Variations in temperatures and effectiveness over time

Figure 5.2 and 5.1 shows the measured temperatures by the thermocouples over-time. The first figure displays the temperatures for a warm supply inlet temperature at 19 °C, and the last displays the temperatures for a cold supply inlet temperature. The blue lines show the temperatures measured by the thermocouples in the supply inlet, while green lines show the temperatures in the supply outlet. The exhaust air is presented with the yellow lines showing the temperatures in the exhaust inlet and the red lines showing the temperatures in the exhaust outlet.

In figure 5.1, the temperatures at each of the openings in the MEE are stable, and the temperatures measured by each of the thermocouples at the same opening are approximately the same. The most substantial gap is the exhaust inlet temperatures, while the supply inlet and exhaust outlet temperatures have a very small difference.

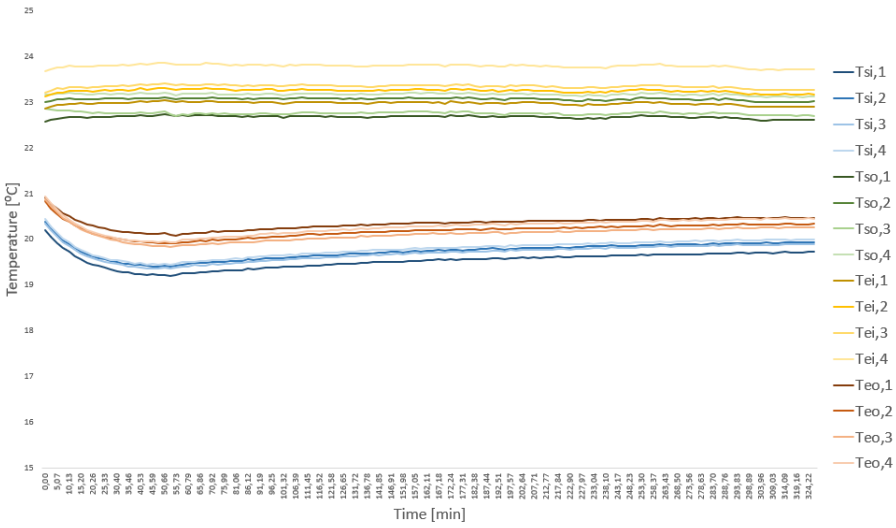

Figure 5.1: The measured temperatures over time with warm outdoor temperature

Figure 5.2 displays how the temperatures in the openings at the MEE changes when the outdoor temperature is cold. In this situation, the temperatures in the exhaust outlet are increasing the temperature gap as the temperature in the opening decreases. However, each of the sensors in the supply inlet measures the same temperatures during the measurement period. The temperature gap suggests that there is a large temperature gradient in the exhaust outlet and that the air is not mixed very well in this opening. The coldest temperatures in this opening are the ones closest to the supply inlet and the cold corner in the exchanger, measured by sensors 3 and 4.

The temperatures close to the warm corner do not display the same temperature gradient as the ones in the cold corner. The warmest temperatures in the supply outlet are measured by sensors 1 and 2 as expected, and the difference between these two temperatures is almost impossible to notice in figure 5.2. The coldest temperature is measured by sensor 3, while the sensor furthest away from the warm corner is the second coldest temperature in this opening.

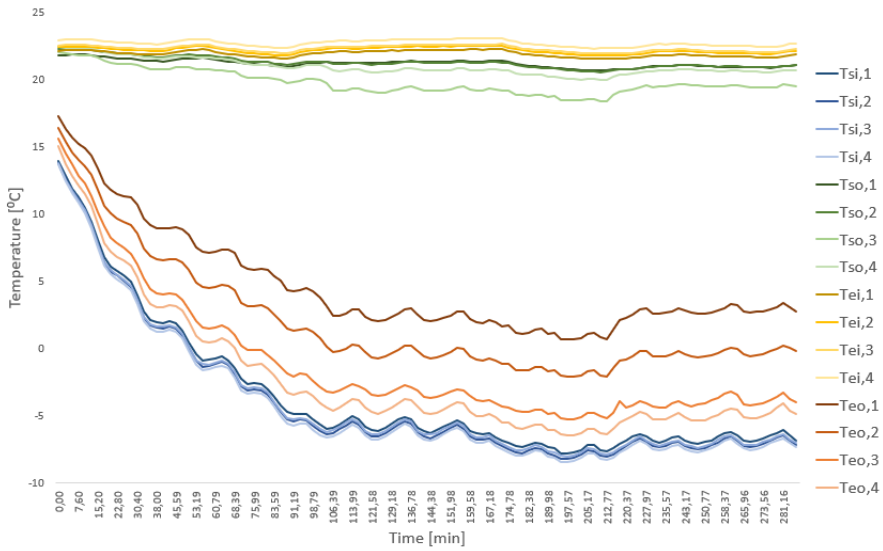

Figure 5.2: The measured temperatures over time with cold outdoor temperature

The sensible effectiveness for the two previous experiments is represented in figure 5.3. Both the effectiveness calculated from the supply side and the effectiveness calculated from the exhaust side are displayed in the figure. Theoretically, the effectiveness should have the same value regardless of which side it is calculated from assuming the ventilation is balanced. However, this is not the case in the figure. When the outdoor temperature is cold, the effectiveness values are much more deviant than expected, which is displayed by the purple lines in the diagram. The effectiveness calculated from the supply side is much higher than the effectiveness values derived from the exhaust side.

The calculated effectiveness at the supply and exhaust side is closer together for warm outdoor temperature.

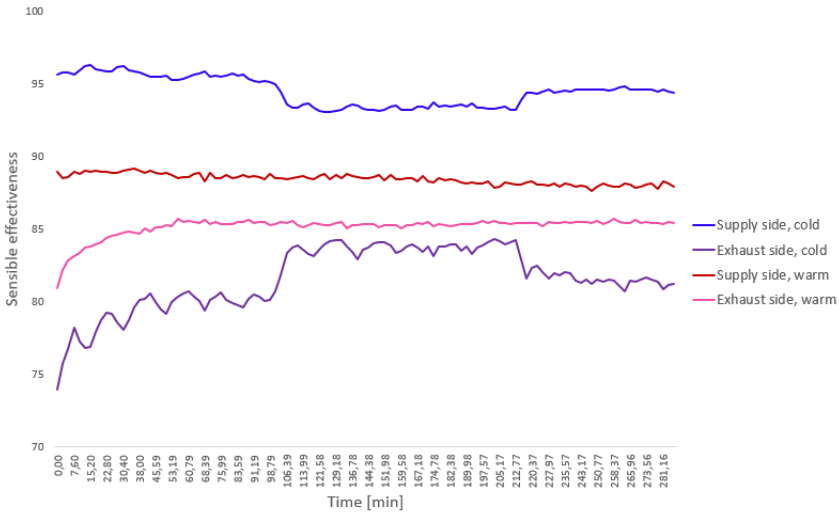

Figure 5.3: Sensible effectiveness over time

Effectiveness results at airflow rate $\dot{V}_1$

Table 5.1 shows the results for the experimental measurements with the airflow rate of $\dot{V} = 4.30$ l/s, which was the lowest of the airflow rates that were tested. The number of measurements is a bit lower for this airflow rate compared to the other two, and this is because it was a little difficult to reach the lowest temperatures that were planned to test. More of the cold temperature is lost in the duct between the cold chamber and the MEE for this airflow rate.

The resulting sensible and latent effectiveness for this airflow rate proved to be very high. The sensible effectiveness values are both higher and closer together than the latent effectiveness values. Since the latent effectiveness has a higher uncertainty, it also makes sense that the values are less consistent. The sensible effectiveness does not seem to be dependent on the outdoor temperature or the exhaust inlet relative humidity based on these values. However, the latent effectiveness seems to have been slightly increased for a higher relative humidity at the same temperature.

Table 5.1: The operating conditions and results for the measurements with $\dot{V} = 4.30$ l/s

Test index	T [$°C$]		$\phi[\%]$		$\dot{V}$[l/s]	$\varepsilon_S[\%]$	$\varepsilon_L[\%]$	P [Pa]
	SI	EI	SI	EI				
0.1	14.5	22.7	40.7	44.4	4.20	95.2	87.8	255
0.5	6.24	22.8	23.0	42.4	4.30	95.2	85.9	254
1.1	-0.32	20.3	16.2	34.4	4.30	95.3	83.7	229
2.1	1.47	22.4	16.8	40.2	4.30	93.1	82.0	240
3.1	2.76	21.8	16.4	49.4	4.10	95.5	85.3	240
4.1	-3.78	21.8	10.2	21.8	4.20	93.5	80.6	244
5.1	-3.73	19.2	11.7	41.0	4.30	96.1	85.1	239
5.2	-4.18	19.9	11.3	43.7	4.30	94.8	83.5	240

Effectiveness at airflow rate $\dot{V}_2$

Table 5.2 shows the results from the conducted measurements with the middle airflow rate at $\dot{V}$ = 6.6 l/s. Test number 6 is missing because the water supply used to regulate the relative humidity was turned off at the time the test was supposed to be conducted. Additionally, the relative humidity values ended up closer than intended for tests 7 and 8.

The resulting sensible effectiveness is a little bit lower than the effectiveness for the lower airflow rate, and there is a bit more variation in the values as well. The latent effectiveness has decreased more than the sensible effectiveness with increasing airflow rate.

Table 5.2: The operating conditions and results for the measurements with $\dot{V} = 6.60$ l/s

Test index	T [$^{\circ}C$]		ϕ[%]		$\dot{V}$[l/s]	ε_S[%]	ε_L[%]	P [Pa]
	SI	EI	SI	EI				
0.1	16.1	22.3	43.0	33.6	6.30	93.6	83.0	422
0.5	4.12	22.7	29.4	42.6	6.40	93.5	78.6	419
1.1	0.43	23.1	24.3	27.4	6.50	93.4	76.5	423
1.2	-0.19	21.7	23.4	30.4	6.60	92.0	76.0	435
1.3	-0.31	21.6	23.7	31.2	6.70	91.6	74.4	445
2.1	-0.04	22.3	21.7	39.1	6.50	92.2	77.1	428
3.1	0.13	19.7	23.0	43.4	6.50	92.5	75.5	431
4.1	-4.22	22.2	16.4	24.0	6.80	94.8	79.0	418
5.1	-4.09	23.0	16.1	34.6	6.50	93.6	77.7	418
7.1	-7.80	22.1	14.4	30.4	6.60	94.7	79.1	421
7.2	-7.03	22.1	15.2	30.9	6.60	94.5	78.6	425
8.1	-8.09	22.1	14.4	31.2	6.60	94.5	79.0	426
8.2	-7.94	23.0	13.1	32.7	6.60	93.1	77.0	425
9.1	-6.05	21.8	15.2	48.4	6.60	94.8	79.8	417

Effectiveness results at airflow rate $\dot{V}_3$

Table 5.3 presents the results from the measurements with $\dot{V}$ = 8.20 l/s, which was the largest airflow rate that was tested. Test number 8 is missing because the water supply regulating the relative humidity was turned off. Instead, test number 7 was conducted three times. Measurement number 2 is presented without the pressure drop, and the airflow rate is assumed. This is because two of the manometers ran out of battery on the same day, and this makes balancing the airflow rates on each side of the exchanger much more uncertain. However, the resulting sensible and latent effectiveness correlate well with the other results, and it was therefore included.

The results for sensible and latent effectiveness are the lowest of the measured values. Once again, there are more variations in the values for latent effectiveness than for sensible effectiveness. However, the sensible effectiveness values are less consistent at this airflow rate compared to the other two. Measurement numbers 5 and 9 stands out with higher sensible effectiveness than the other, while measurement 0.1 and 4 stand out with low values. Test number 4 also has the lowest measured latent effectiveness, which is a considerably lower value than the rest.

Table 5.3: The operating conditions and effectiveness for $\dot{V} = 8.20$l/s

Test index	T [$^{\circ}C$]		ϕ[%]		$\dot{V}$[l/s]	ε_S[%]	ε_L[%]	P [Pa]
	SI	EI	SI	EI				
0.1	19.9	23.3	44.5	47.7	7.90	88.1	73.8	556
0.2	16.1	23.0	48.5	45.0	8.00	92.4	76.9	567
0.3	14.9	22.3	48.2	45.3	8.00	92.8	77.9	566
0.5	4.44	22.7	34.0	40.5	8.10	93.2	76.3	563
1.1	-1.30	21.6	21.2	24.5	8.20	92.9	73.3	565
1.2	-0.55	23.0	26.0	27.9	8.20	93.3	74.5	557
2.1	0.18	20.1	25.8	40.0	8.20*	92.3	74.5	
3.1	-1.42	21.2	21.0	49.8	8.20	92.1	74.9	556
4.1	-4.24	21.5	20.8	21.8	8.20	88.6	67.2	558
5.1	-4.56	19.2	19.1	39.7	8.20	95.2	76.7	552
6.1	-4.41	22.8	19.8	50.7	8.20	92.3	75.5	562
7.1	-8.83	21.2	17.8	26.1	8.30	91.6	71.6	561
7.2	-9.15	21.4	17.6	28.7	8.30	92.9	74.4	571
7.3	-10.5	21.7	15.1	27.4	8.20	91.1	71.4	566
9.1	-6.87	21.6	16.1	48.1	7.80	94.3	77.6	543

*Airflow rate is assumed

5.2 Frost formation

Frost formation in the exhaust air stream was only experienced when both the temperature was at its coldest and the indoor relative humidity was high, at T_3 and φ_3. None of the experiments displayed a complete blockage of the exhaust outlet due to frost formation. However, the endoscope used to discover the frost gave unclear displays, and the frost was difficult to notice.

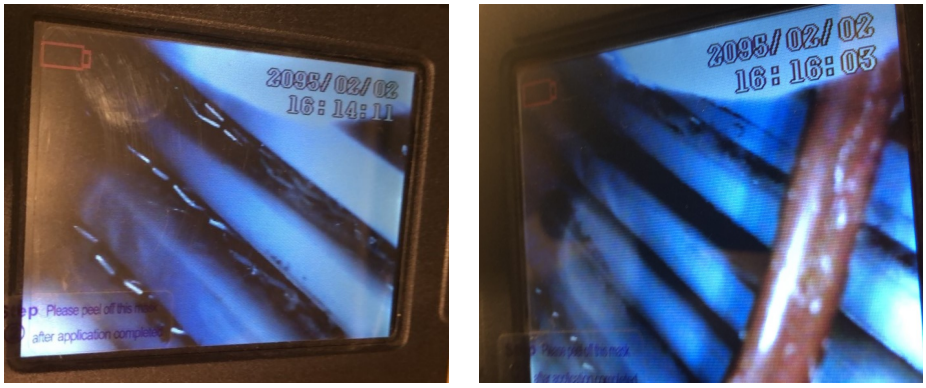

(a) Without frost formation **(b)** With some frost formation

Figure 5.4: Close view of the exhaust outlet without and with some frost formation

Figure 5.4 present pictures of the exhaust outlet taken in a close view, only showing parts of the opening. No frost could be detected in the figure to the left, but some can be seen in the figure to the right. Figure 5.5 shows how the endoscope displayed the exhaust outlet when more of the opening is included in the frame. As seen in the figure, it is difficult to determine if there are any frost formation in this picture. To be able to determine frost formation, the endoscope had to get a closer view.

Figure 5.5: The exhaust outlet seen further away

Each experiment lasted between 5.5-7 hours. If the exchanger were given more time, perhaps frost in more of the experiments would have been detected. There could have been some frost that was not discovered, but there was definitely no complete blockage for any of the experiments. Additionally, the expected pressure rise on the exhaust side as a result of frost formation was not detected for any of

the measurements.

5.3 Pressure drop

Figure 5.6 shows the pressure drops for all the conducted experiments. The pressure drops were measured with manometers, and therefore, the number of measurements for each point is lower than for the effectiveness measurements. Instead, the pressure drops were written down a few times for each experiment, and the point marked in the figure is the average of these.

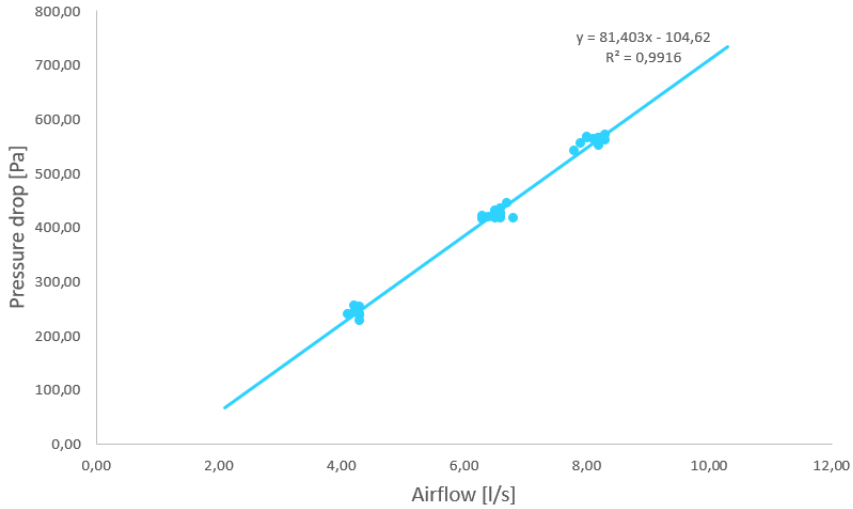

Figure 5.6: The measured pressure drops

As clearly seen in the figure, the pressure drops increase linearly with increasing airflow rate. The pressure drop follows the trend line given in the equation below with the accompanying R^2-value:

$$\Delta P = 81.4\dot{V} - 104$$
$$R^2 = 0.99$$

The measured pressure drops at the same airflow rate are approximately the same, and only a few of the points deviate a little from the line.

5.4 VOC transfer through the MEE

This section contains the results from the formaldehyde transfer experiments. To make a comparison between the experiments easier, only the main results are presented in this section. More detailed results for each of the individual measurements, some initial measurements, and larger graphs are given in Appendix A5.

Some initial measurements with the formaldehyde sensors were conducted before the particleboard was included, which is described in detail in Appendix A5. This was done to establish the external formaldehyde concentrations in the laboratory and in the cold chamber. The results showed that the concentrations in the laboratory room during work hours was unstable and could get quite large, probably as a result of other work conducted in the lab. To avoid too much external impact, the experiments were mainly carried out during the evenings and weekends.

Table 5.4: The average exhaust air transfer rates

Test index	T[°C]			φ [%]			$\dot{V}$[l/s]	EATR[%]
	SI	SO	EI	SI	SO	EI		
1	14.5	22.3	22.7	40.7	43.0	44.4	4.2	55.0
2	16.1	21.9	22.3	43.0	33.7	33.6	6.3	29.3
3	14.9	21.8	22.3	48.2	43.4	45.3	8.0	51.1
4	6.24	22.0	22.8	23.0	39.5	42.4	4.3	50.5
5	4.12	21.5	22.7	29.4	38.1	42.6	6.4	48.3
6	4.44	21.4	22.7	34.0	36.0	46.9	8.1	52.1
2.2	15.1	21.9	22.4	56.7	40.3	39.5	6.3	41.0
3.2	16.1	22.5	23.0	48.5	43.2	45.0	8.0	93.8

Table 5.4 presents the average values for each of the experiments for the period the particleboard was placed in the exhaust inlet. The operating conditions at the openings where the sensors were placed are given, and the average exhaust air transfer rates are calculated. Test number 2.2 and 3.2 are repeated measurements of test number 2 and 3, respectively. The average values for the repeated measurements do not correlate particularly well, although test number 2 and 2.2 are the two with the lowest average value. Test number 3.2 stands out with an unusually high average EATR value.

Formaldehyde transfer for the warm supply temperature

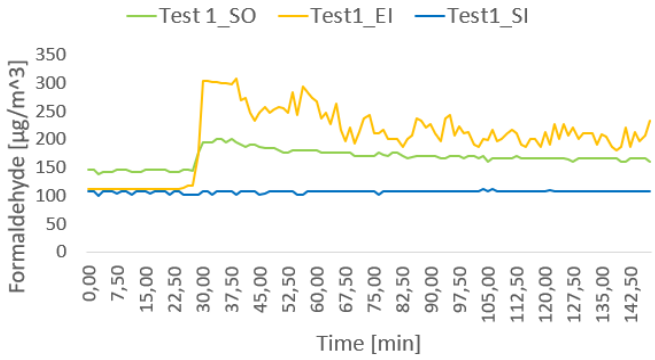

(a) Test 1

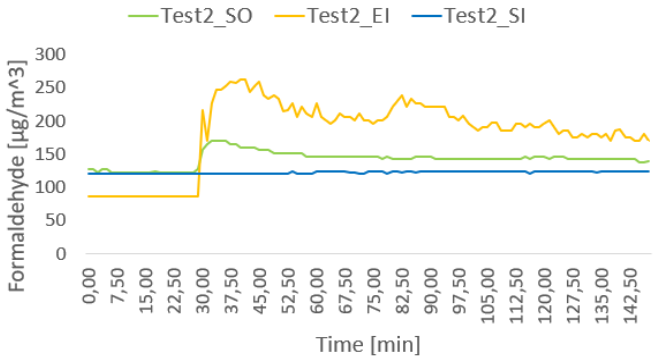

(b) Test 2

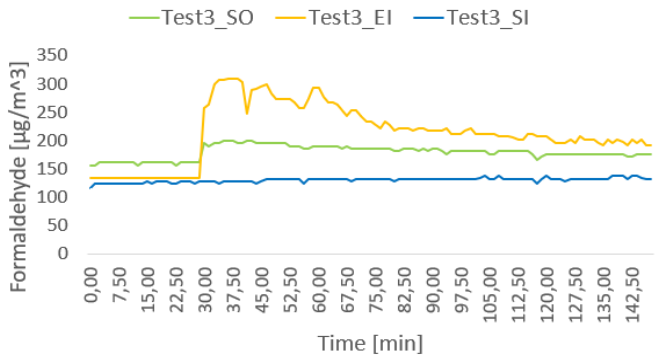

(c) Test 3

Figure 5.7: The formaldehyde concentrations over time for test 1-3

Figure 5.7 shows the formaldehyde concentrations over time measured by each of the sensors for test number 1, 2, and 3. Each of these experiments had an outdoor temperature of approximately 15 °C. The blue lines represent the concentrations measured in the cold chamber by the duct inlet. The green lines show the concentrations in the supply outlet, and the yellow line represents the concentrations in the exhaust inlet.

In each of the experiments, the particleboard was placed by the exhaust inlet 30 minutes after the graph time count starts, which can be seen clearly by the step response at the exhaust inlet. The supply outlet concentrations follow the exhaust inlet with a smaller step response, suggesting that some of the formaldehyde is transferred through the membrane. Nevertheless, this transfer was more substantial than expected for all of the experiments compared to the literature.

Test number 1 was carried out for the smallest airflow rate, test 2 was for the medium airflow rate, and test 3 was with the largest airflow rate. There was not a very noticeable trend for increasing airflow rate, and the transfer of formaldehyde seems to be almost independent of the airflow rate. Yet, the step in the supply outlet when the particleboard was inserted seems to be slightly larger for test 1. Test 3 seems to have the smallest increase in the supply outlet, and this could, therefore, mean that the exhaust transfer is a bit larger at lower airflow rates.

There were several differences between the experiments. Test number 2 had higher concentrations of formaldehyde in the cold chamber and at the exhaust outlet than in the exhaust inlet. This could be because the concentrations in the cold chamber were higher that day. Test number 1 and test number 3 were carried out the same day, and the concentrations in the cold chamber were similar for these two experiments.Both of these two experiments had a gap between the supply outlet and the other two lines before the particleboard was placed. This gap could be a result of either a formaldehyde source inside the MEE, that the sensors included some source in the surrounding air, or uncertainties in the measurements from the sensors.

Formaldehyde transfer for the cold supply temperature

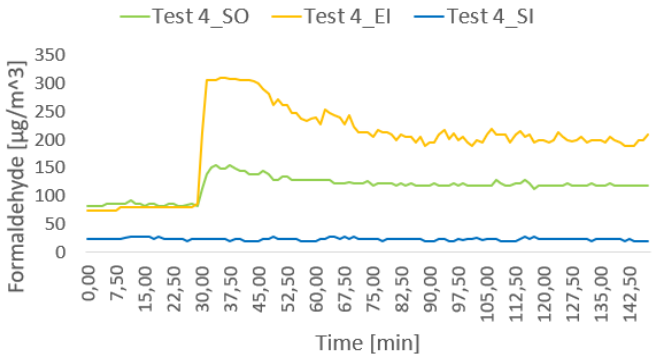

(a) Test 4

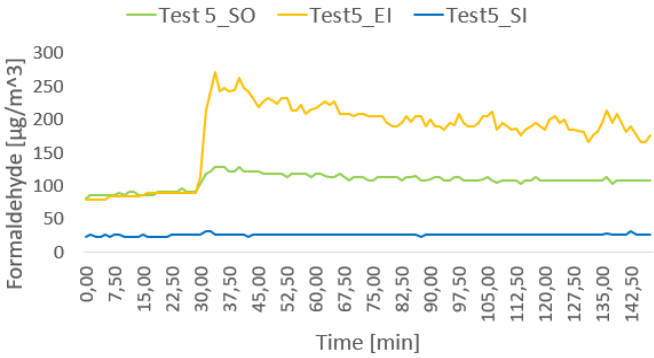

(b) Test 5

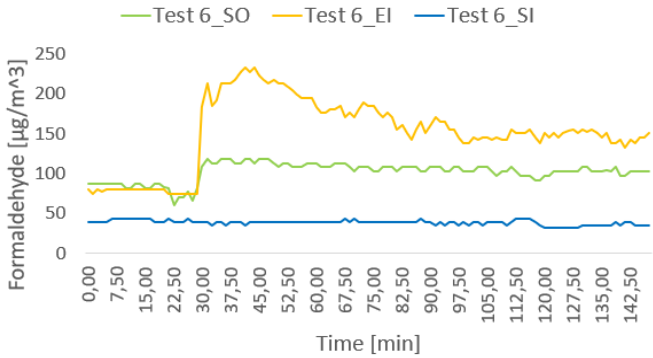

(c) Test 6

Figure 5.8: The formaldehyde concentrations over time for test 4-6

Figure 5.8 shows the formaldehyde concentrations over time for test number 4-6. Once again, the blue line represents the cold chamber; the green line represents the supply outlet and the yellow line the exhaust inlet. These experiments were conducted with a lower outdoor temperature at approximately 5 °C. Test number 4 was carried out with the low airflow rate, test number 6 with the high airflow rate and test number 5 with the airflow rate in the middle. The sensors in the supply outlet and the exhaust inlet had switched place for these experiments compared to test numbers 1-3.

Similarly to the previous tests, the most significant step in the supply outlet is observed for the measurement with the lowest airflow rate. However, the other two measurements had approximately the same difference measured at the supply outlet. These results slightly support the hypothesis that the exhaust air transfer rates decrease with increasing airflow rate.

One thing these tests have in common compared to the previous tests is that there is no longer any gap between the supply outlet and the exhaust inlet before the particleboard insertion. This could be a result of switching the two sensors since the exhaust outlet was larger for all the previous tests.

Perhaps the most noticeable difference for test 4-6 compared to the previous tests is the concentrations measured in the cold chamber. The measured concentrations in the cold chamber are much lower for test 4-6 compared to previously, and the only apparent explanation is the difference in the outdoor temperature. While the outdoor temperature in the MEE is approximately 5 °C for these experiments, the temperature is in reality between -7 °C and -5 °C in the cold chamber where the sensor is located. This is because some of the cold temperature is lost in the duct from transporting the air from the cold chamber to the MEE.

Repeat of experiment 2 and 3

Figure 5.9 display measurements number 2.2 and 3.2, which are repeated measurements of test number 2 and 3, respectively. The only difference between the first tests and the repeated tests is that the placement of sensors in the supply outlet and in the exhaust inlet were switched.

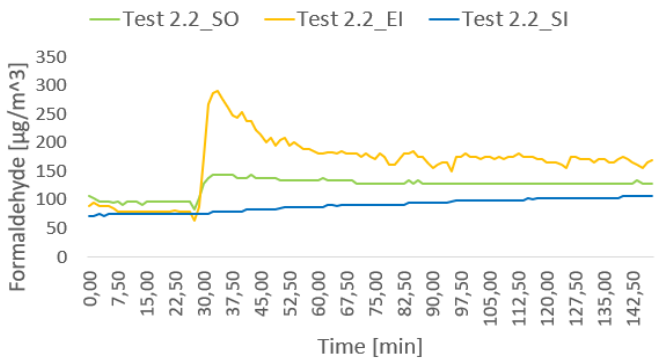

(a) Test 2.2

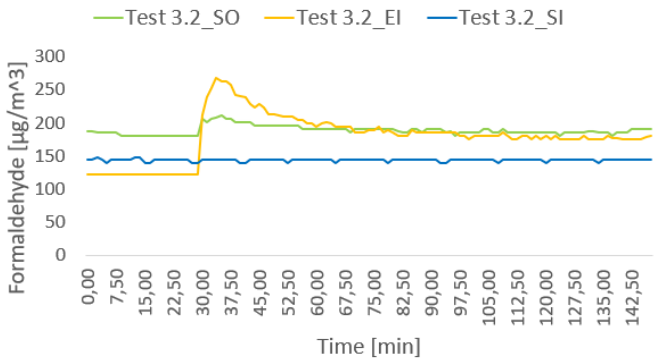

(b) Test 3.2

Figure 5.9: The formaldehyde concentrations over time for the repeat of test 2 and 3

Test 2.2 has a small gap between the measured concentrations in the cold chamber and the supply outlet before the particleboard is placed at the exhaust inlet compared to the previous test 2. However, the gap is not larger compared to the other tests at the same temperature. This measurement is the only one where the concentration in the cold chamber increases slightly with time. The test was conducted later during the day after test number 5, so the temperature in the cold chamber had been approximately 15 ° C colder a few hours earlier. Since the test results with the colder supply temperature suggest that the sensor is affected by the cold temperatures, this could still be the case for this measurement.

Test 3.2 has a somewhat higher initial concentration in the exhaust inlet, and substantially higher initial concentration in the supply outlet and the cold chamber compared to all the other conducted experiments. The gap in the initial period between the concentrations in the supply outlet and the concentrations in the cold

chamber is larger for this measurement than the others at the same temperature as well. The immense concentration in the supply outlet results in a very high EATR value.

Chapter 6

Discussion

The discussion evaluates the main findings from the previous chapter. Results from the effectiveness measurements and the formaldehyde measurements are compared with literature. The test rig used for measurements is evaluated as well.

6.1 Evaluation of the test rig

The test rig, including the MEE core, had not been in use for a few years, and the rig was built quite a few years ago. There could have been a degradation in the performance, e.g., more air leakages. The ducts were investigated with regards to air leakages with air supplied in the ducts, but the air was still warmed up quite a lot from the cold chamber till it reached the MEE.

The cold chamber had been upgraded since previous experiments had been conducted with the test rig. Although the temperature in the cold chamber was supposed to be constant, it could, in reality, vary with $\pm 1^{\circ}$C. The supplied temperature could, therefore, have slight variations when the exchanger was supposed to be in steady-state. Additionally, the two evaporators sometimes went into an anti-freezing mode. The evaporators were set to go into anti-freezing mode at different times, but a few times during the first couple of experiments, they turned on anti-freeze at the same time. The air could then be warmed up a little during the time the evaporators were set to anti-freeze.

6.2 Effectiveness measurements

Comparison of the conducted experiments

The results showed that both the latent and the sensible effectiveness decreased with increasing airflow rate. All of the effectiveness measurements are displayed in figure 6.1 only in relation to the airflow rate. As seen in the figure, both the sensible effectiveness and the latent effectiveness decreases with increasing airflow rate. The latent effectiveness decreases more rapidly than the sensible effectiveness, and decrease in the sensible effectiveness was not as significant as expected.

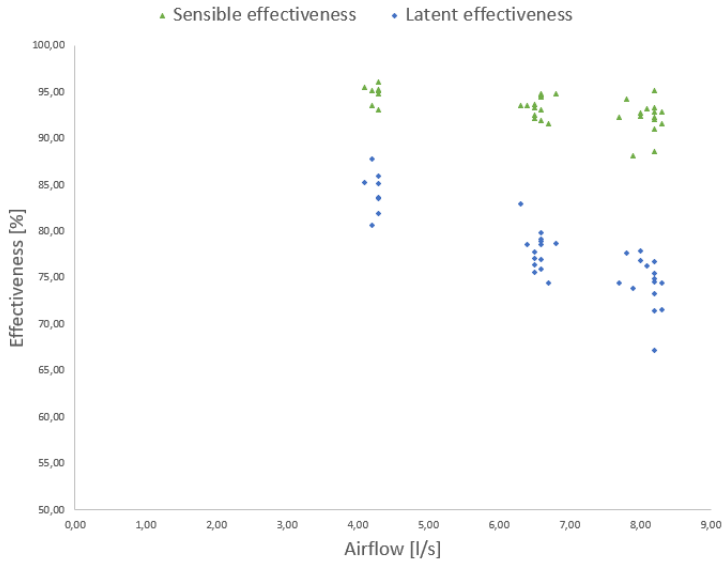

Figure 6.1: All of the effectiveness measurements plotted in one figure

The latent effectiveness measurements had higher uncertainty than the effectiveness values, so it was anticipated that the measurements would be more divergent than the sensible effectiveness. Additionally, the latent effectiveness can be dependent on more than just the airflow rate [23]. The sensible effectiveness, however, had surprisingly divergent results at the largest airflow rate.

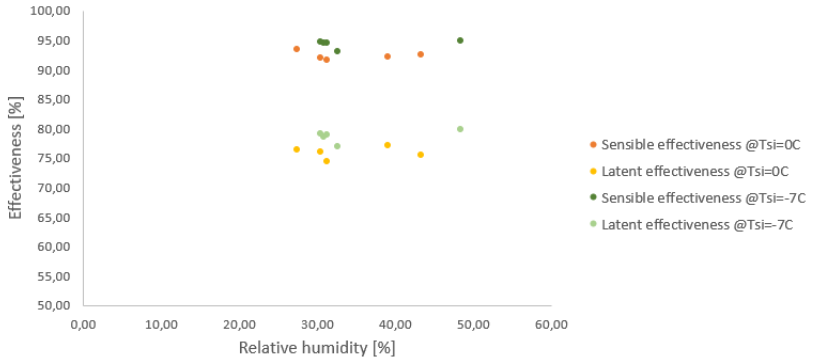

Figure 6.2: The measures sensible and latent effectiveness for two temperature and with $\dot{V}$ = 6.6 l/s

Figure 6.2 displays the results at airflow rate 6.6 l/s for two different temperatures. According to [23], the latent effectiveness should be less for higher temperatures. This is consistent with the graph as the green dots represent the lowest temperature. The sensible effectiveness was also higher at the lower temperature in this case, which was not expected.

Reasons for inconsistencies in the measurements

Inconsistencies in the measured effectiveness could be a result of different reasons. The following paragraphs describe the possible reasons for this.

Although the calculated airflow rates on each side gave the same value, the real airflow rates would actually not be the same. Unbalanced airflow rates could lead to increased effectiveness. The effectiveness values were, in fact, not equal when calculated from the supply side compared to the exhaust side.

The airflow rates were based on the calculations made after measuring the pressure difference over the orifice plates. These calculations were also affected by the density of the air, which again depended on the temperature. The temperatures that were used were the ones measured close to the supply inlet and the exhaust outlet. These temperatures were some distance away from the orifice plates. There could have been some temperature loss in the duct from the exhaust outlet to the orifice plate, and from the orifice plate to the supply inlet.

Another reason why the effectiveness calculated from the exhaust side and the supply side gave different results could be the temperature distribution in the MEE. The temperatures measured by the four thermocouples in the exhaust outlet gave

significantly different values. To calculate the effectiveness from the exhaust side, the average of these measured values was used. Compared to the effectiveness measured by Peng Liu [15], the effectiveness values measured from the supply side seemed most accurate.

Furthermore, all of the measurements include some uncertainty, and the uncertainty could result in variations of the results. The resulting uncertainty was found to be higher for latent effectiveness than sensible. When the total uncertainties for the effectiveness were calculated, the airflow rate was assumed to be constant, and the uncertainty of the airflow rate was not included.

The last possible reason is that the membrane could have unknown deficiencies. Since the MEE had not been tested for a long time, the membrane could have been broken. The large exhaust air transfer ratios of formaldehyde indicate that the membrane could have deficiencies.

6.3 VOC transfer through the MEE

EATR values compared to the concentration graphs

The VOC transfer through the exchanger was higher than expected. The average EATR was between 29.3 % and 93.8 % for the experiments. When the outdoor temperature was low, the sensors were assumed to show too low concentrations in the cold chamber. Additionally, the formaldehyde concentrations in the cold chamber were sometimes higher than the laboratory room. Both of these affect the calculated EATR value and can give results that are too high.

The graphs given in the result chapter of the formaldehyde concentrations in each of the openings provides more information than the EATR values. The increased concentration measured in the supply outlet at the time the particleboard was placed in the exhaust inlet, was found to be more significant than expected for all of the measurements.

The sensors are new, and the uncertainty of the sensors is unknown. Uncertainty in the measurements could be added by the chosen placement of the sensors. Ideally, the sensors should have been placed close to the exchanger openings by the thermocouples. Instead, they had to be placed outside of the duct because of the size of the sensor rigs. Regardless of uncertainty from the sensors, the transfer of formaldehyde was found to be higher than desired.

Evaluation of the membrane material regarding VOC transfer

Compared to the literature [34, 35, 36], the detected formaldehyde transfer to the supply air was higher than expected. The investigated MEE used a polypropylene membrane, and polypropylene membranes were one of the materials with the least selectivity to water over other species according to the previous studies. The previous studies also stated that the selectivity of different membranes could vary greatly depending on the membrane material.

The membranes that were in a glassy state generally had a higher selectivity to water over other species than membranes in a rubbery state. Membranes in a rubbery state, on the other hand, generally showed a higher moisture permeability according to a previous study [36]. If the statement is correct, then the latent effectiveness could be reduced if the membrane was chosen solely based on minimising the EATR.

EATR values for membrane energy exchangers need further studies. If the evaluated MEE is considered for use in buildings where it is essential to avoid too much transfer of contaminants, then a membrane with higher selectivity to water would be preferable. An acceptable limit for EATR values regarding MEEs for its general use should be decided, and the EATR evaluated when the membrane material for a given MEE is chosen.

Chapter 7

Conclusion

A membrane energy exchanger prototype has been experimentally investigated regarding effectiveness, pressure drop, and VOC transfer. The effectiveness was measured for different airflow rates, outdoor temperatures, and indoor relative humidity. The transfer of formaldehyde through the MEE was measured for different airflow rates and outdoor temperatures.

The results showed that both the sensible and the latent effectiveness were quite high. Values between 88.1% and 96.1% were measured for the sensible effectiveness, and values between 87.8% and 67.2% were measured for the latent effectiveness. The highest average values were experienced for the lowest airflow rate, and the lowest average values were experienced for the largest airflow rates.

Inconsistencies in the measured effectiveness were found to possibly be a result of one or more of the following explanations:

- Although the calculated airflow rates on each side gave the same value, the real airflow rates would actually not be the same. Unbalanced airflow rates could lead to increased effectiveness.
- All of the measurements include some uncertainty, and the resulting uncertainty is higher for the latent effectiveness than the sensible. The calculated uncertainty for the effectiveness values was based on the assumption that the airflow rates were equal, and the real uncertainty could be larger.
- The membrane could have unknown deficiencies.

The VOC transfer through the exchanger was higher than expected. The average EATR between 29.3 % and 93.8 % proved not to be useful for evaluation of the

VOC transfer. When the outdoor temperature was low, the sensors were assumed to show too low concentrations in the cold chamber. Additionally, the formaldehyde concentrations in the cold chamber were sometimes higher than the laboratory room. Both of these affect the calculated EATR value.

Regardless of uncertainty from the sensors, the transfer of formaldehyde was found to be higher than desired. The investigated MEE used a polypropylene membrane, and polypropylene membranes were one of the materials with the least selectivity according to previous studies.

If the evaluated MEE is considered for use in buildings where it is essential to avoid too much transfer of contaminants, then a membrane with higher selectivity to water would be preferable.

Chapter 8

Further work

A membrane energy exchanger has been experimentally investigated related to effectiveness and exhaust air transfer of contaminants. This type of heat exchanger is still relatively new for many, and there are several opportunities for further studies.

As the membrane exchanger is still relatively new, not many studies have focused on the long term performance and the lifetime of MEEs. Additionally, the long term performance and durability of different membrane materials should be investigated.

To make sure the MEE is suitable for residential buildings with several living units, other types of membranes with higher selectivity of moisture over formaldehyde should be tested. Other types of VOCs and gases such as CO_2 could also be investigated.

Performance of MEE in climates or seasons which are neither cold and dry nor hot and humid. Countries with cold and dry winters would usually want to use a ERV during the spring and fall seasons as well.

Bibliography

[1] Maren Evensen. Analysis of membrane based heat exchanger for ventilation, 2019.

[2] IPCC. Climate change 2014: Synthesis report. contribution of working group i, ii and iii to the fifth assessment report of the intergovernmental panel on climate change [core writing team, r. k. pachauri and l. a. meyers], 2014.

[3] UN environment and International Energy Agency. Towards a zero-emission, efficient, and resilient buildings and construction sector. global status report 2017., 2017.

[4] A P Jones. Indoor air quality and health. *Atmospheric Environment*, 33(28):4535–4564, 1999.

[5] SINTEF NTNU. *Enøk i bygninger - Effektiv energibruk*. Gyldendal undervisning, 3rd edition, 2007.

[6] Direktoratet for byggkvalitet. Tek17: Byggteknisk forskrift, 2017.

[7] S. Ingebrigtsen. *Ventilasjonsteknikk Del 1*. Skarland Press AS, 2015.

[8] Mohammad Rafati Nasr, Melanie Fauchoux, Robert W Besant, and Carey J Simonson. A review of frosting in air-to-air energy exchangers. *Renewable and Sustainable Energy Reviews*, 30:538–554, 2014.

[9] Jesper Kragh, Jørgen Rose, and Svend Svendsen. *Mechanical ventilation with heat recovery in cold climates*. 2005.

[10] Li-Zhi Zhang. Heat and mass transfer in a quasi-counter flow membrane-based total heat exchanger. *International Journal of Heat and Mass Transfer*, 53(23):5478–5486, 2010.

[11] A. Mardiana-Idayu and S. B Riffat. Review on heat recovery technologies for building applications. *Renewable and Sustainable Energy Reviews*, 16:1241–1255, 2012.

[12] Cheng Zeng, Shuli Liu, and Ashish Shukla. A review on the air-to-air heat and mass exchanger technologies for building applications. *Renewable and Sustainable Energy Reviews*, 75:753–774, 2017.

[13] *2008 ASHRAE Handbook - Heating, Ventilating and Air-Conditioning Systems ans Equipment (I-P Edition)*. American Society of Heating, Refrigerating and Air-Conditioning Engineers, Inc (ASHRAE), 2008.

[14] Yunus A. Cengel and Michael A. Boles. *Thermodynamics: An Engineering Approach*. McGraw-Hill, 5 edition, 2006.

[15] Peng Liu, Maria Justo Alonso, Hans Martin Mathisen, and Carey Simonson. Performance of a quasi-counter-flow air-to-air membrane energy exchanger in cold climates. *Energy and Buildings*, 119:129–142, 2016.

[16] J L Niu and L Z Zhang. Membrane-based Enthalpy Exchanger: material considerations and clarification of moisture resistance. *Journal of Membrane Science*, 189(2):179–191, 2001.

[17] T. L. Bergman F. P. Incropera, D. P. Dewitt and A. S. Lavine. *Priciples of Heat and Mass Transfer*. John Wiley & Sons Singapore, 7th edition, 2013.

[18] W. M. Kays and A. L. London. *Compact Heat Exchangers*. McGraw-Hill Book Company, 1984.

[19] L Z Zhang and J L Niu. Effectiveness Correlations for Heat and Moisture Transfer Processes in an Enthalpy Exchanger With Membrane Cores. *Journal of Heat Transfer*, 124(5):922–929, 2002.

[20] Jingchun Min and Jiangfei Duan. Comparison of various methods for evaluating the membrane-type total heat exchanger performance. *International Journal of Heat and Mass Transfer*, 100:758–766, 2016.

[21] Václav Dvořák and Tomáš Vít. CAE methods for plate heat exchanger design. *Energy Procedia*, 134:234–243, 2017.

[22] Jingchun Min and Ming Su. Performance analysis of a membrane-based energy recovery ventilator: Effects of membrane spacing and thickness on the ventilator performance. *Applied thermal engineering*, 30:991–997, 2010.

[23] Jingchun Min and Ming Su. Performance analysis of a membrane-based energy recovery ventilator: Effects of outdoor air state. *Applied Thermal Engineering*, 31:4036–4043, 2011.

[24] Jason Woods. Membrane processes for heating, ventilation, and air conditioning. *Renewable and Sustainable Energy Reviews*, 33:290–304, 2014.

[25] Li-Zhi Zhang, Yuan-Yuan Wang, Cai-Ling Wang, and Hui Xiang. Synthesis and characterization of a pva/licl blend membrane for air dehumidification. *Journal of Membrane Science*, 308:198–206, 2008.

[26] Li-Zhi Zhang. *Conjugate Heat and Mass Transfer in Heat Mass Exchanger Ducts*, chapter 2. Academic Press, Elsevier Inc, 2014.

[27] United States Environmental Protection Agency. Volatile organic compounds' impact on indoor air quality, 2017.

[28] Md. Aynul Bari, Warren B. Kindzierski, Amanda J. Wheeler, Eve Héroux, and Lance A. Wallace. Source apportionment of indoor and outdoor volatile organic compounds at homes in edmonton, canada. *Building and Environment*, 90:114–124, 2015.

[29] Aziz Khanchi, Christopher A. Hebbern, Jiping Zhu, and Sabit Cakmak. Exposure to volatile organic compounds and associated health risks in windsor, canada. *Atmospheric Environment*, 120:152–159, 2015.

[30] WHO Regional Office for Europe. Who guidelines for indoor air quality: selected pollutants, 2010.

[31] ANSI/AHRI Standard 1060 (I-P). 2014 standard for performance rating of air-to-air exchanger for energy recovery ventilation equipment, 2015.

[32] Hiren Patel, Gaoming Ge, Mohamed R. H. Abdel-Salam, Ahmed H. Abdel-Salam, Robert W. Besant, and Carey J. Simonson. Contaminant transfer in run-around membrane energy exchangers. 70:94–105, 2014.

[33] Erin L. Hult, Henry Willem, and Max H. Sherman. Formaldehyde transfer in residential energy recovery ventilators. *Building and Environment*, 75:92–97, 2014.

[34] Ryan Huizing, Hao Chen, and Frankie Wong. Contaminant transport in membrane based energy recovery ventilators. *Science and Technology for the Built Environment*, 21:54–66, 2015.

[35] L. Z. Zhang, X. R. Zhang, Q. Z. Miao, and L. X. Pei. Selective permeation of moisture and vocs through polymer membranes used in total heat exchangers for indoor air ventilation. *Indoor Air*, 22:321–330, 2012.

[36] Amin Engarnevis, Sarah Romani, Alexander Sylvester, Ryan Huizing, Sheldon Green, and Steven Rogak. The effects of temperature and humidity on the permeation properties of membrane transport media used in energy recovery ventilators. 2017.

[37] L. Z. Zhang. Laminar flow and heat transfer in plate-fin triangular ducts in thermally developing entry region. *International journal of heat and mass transfer*, 50:1637–1640, 2007.

[38] Jason Woods and Eric Kozubal. Heat transfer and pressure drop in spacer-filled channels for membrane energy recovery ventilators. *Applied Thermal Engineering*, 50(1):868–876, 2013.

[39] Gazi I Mahmood, Carey J Simonson, and Robert W Besant. Experimental Pressure Drop and Heat Transfer in a Rectangular Channel With a Sinusoidal Porous Screen. *Journal of Heat Transfer*, 137(4):042601–042601, 2015.

[40] Peng Liu, Hans Mathisen, Maria Justo Alonso, and Carey Simonson. A frosting limit model of air-to-air quasi-counter-flow membrane energy exchanger for use in cold climates. 111:776–785, 2017.

[41] Ns-en iso 5167-1: Measurement of fluid flow by means of pressure differential devices inserted in circular cross-section conduits running full - part 1: General principles and requirements (iso 5167-1:2003), 2003.

[42] Ns-en iso5167: Measurement of fluid flow by means of pressure differential devices inserted in circular cross-section conduits running full - part 2: Orifice plates (iso 5167-2:2003), 2003.

[43] DPM. Dpm tt 570 micromanometer 1 pascal resolution.

[44] Vaisala. Hmt330 series humidity and temperature transmitters - for demanding humidity measurement, 2018.

[45] Peng Liu. *Energy Recovery with Air-to-air Membrane Energy Exchanger for Ventilation in Cold Climates*. PhD thesis, NTNU, 2016.

[46] Ltd ProSense Technologies Co. Dart sensors wz-s formaldehyde module - operation manual.

[47] SN/K 094. Ns-en 13986:2004 + a1:2015, wood-based panels for use in construction - characteristics, evaluation of conformity and marking, 2015.

[48] Hugh W. Coleman and W. Glenn Steele. *Experimentation, Validation, and uncertaity analysis for engineers*. John Wiley Sons, INC, third edition, 2009.

Appendix

Appendix A1: Risk assessment report

Appendix A2: Equipments and components

Appendix A3: Equipment used in VOC measurements

Appendix A4: Results: Effectiveness measurements

Appendix A5: Results: Formaldehyde measurements

Appendix A1
Risk assessment report

NTNU HSE	Hazardous activity identification process	Prepared by	Number	Date
		HSE section	HMSRV2601E	09.01.2013
		Approved by		Replaces
		The Rector		01.12.2006

Unit: *EPT* **Date: 02.03.2019**

Line manager: Terese Løvås

Participants in the identification process (including their function)**:**

Short description of the main activity/main process: Master project for student xx. Performance of membrane energy exchanger

Is the project work purely theoretical? (YES/NO): NO *Answer "YES" implies that supervisor is assured that no activities requiring risk assessment are involved in the work. If YES, briefly describe the activities below. The risk assessment form need not be filled out.*

Signatures: *Responsible supervisor:* *Student:*

ID nr.	Activity/process	Responsible person	Existing documentation	Existing safety measures	Laws, regulations etc.	Comment
	Running effectiveness experiments at the membrane energy exchanger test rig	Maren	No	No	No	

NTNU HSE/KS	Risk assessment	Prepared by	Number	Date
		HSE section	HMSRV2603E	04.02.2011
		Approved by		Replaces
		The Rector		01.12.2006

Unit: *EPT* **Date: 02.03.2019**

Line manager: Terese Løvås

Participants in the identification process (including their function)**:**

Short description of the main activity/main process: Master project for student xx. Performance of membrane energy exchanger

Signatures: *Responsible supervisor:* *Student:*

Activity from the identification process form	**Potential undesirable incident/strain**	**Likelihood:**	**Consequence:**			**Risk Value (human)**	**Comments/status Suggested measures**
		Likelihood (1-5)	Human (A-E)	Environment (A-E)	Economy/ material (A-E)		
Running effectiveness experiments at the membrane energy exchanger test rig	Leakage of cold air from the supply air pipes	2	A	A	A	A2	The responsible person should wear gloves if there is a need to touch cold surfaces.
Running effectiveness experiments at the membrane energy exchanger test rig	Water leakage from the air container	3	A	A	A	A3	Make sure the fans and the water supply is shut off before opening the door.
Running effectiveness experiments at the membrane energy exchanger test rig	The humidifier is out of water, and the temperature increases. This could cause a fire.	2	A	A	C	A2	Make sure that there is enough water at the beginning of the experiment. Check that the thermostats and safety measures works properly.

Likelihood, e.g.:
1. *Minimal*
2. *Low*
3. *Medium*
4. *High*
5. *Very high*

Consequence, e.g.:
A. *Safe*
B. *Relatively safe*
C. *Dangerous*
D. *Critical*
E. *Very critical*

Risk value (each one to be estimated separately):
Human = Likelihood x Human Consequence
Environmental = Likelihood x Environmental consequence
Financial/material = Likelihood x Consequence for Economy/materiel

Potential undesirable incident/strain

Identify possible incidents and conditions that may lead to situations that pose a hazard to people, the environment and any materiel/equipment involved.

Criteria for the assessment of likelihood and consequence in relation to fieldwork

Each activity is assessed according to a worst-case scenario. Likelihood and consequence are to be assessed separately for each potential undesirable incident. Before starting on the quantification, the participants should agree what they understand by the assessment criteria:

Likelihood

Minimal 1	Low 2	Medium 3	High 4	Very high 5
Once every 50 years or less	Once every 10 years or less	Once a year or less	Once a month or less	Once a week

Consequence

Grading	Human	Environment	Financial/material
E Very critical	May produce fatality/ies	Very prolonged, non-reversible damage	Shutdown of work >1 year.
D Critical	Permanent injury, may produce serious serious health damage/sickness	Prolonged damage. Long recovery time.	Shutdown of work 0.5-1 year.
C Dangerous	Serious personal injury	Minor damage. Long recovery time	Shutdown of work < 1 month
B Relatively safe	Injury that requires medical treatment	Minor damage. Short recovery time	Shutdown of work < 1week

A **Safe**	Injury that requires first aid	Insignificant damage. Short recovery time	Shutdown of work < 1day

The unit makes its own decision as to whether opting to fill in or not consequences for economy/materiel, for example if the unit is going to use particularly valuable equipment. It is up to the individual unit to choose the assessment criteria for this column.

Risk = Likelihood x Consequence
Please calculate the risk value for “Human”, “Environment” and, if chosen, “Economy/materiel”, separately.

About the column ”Comments/status, suggested preventative and corrective measures”:
Measures can impact on both likelihood and consequences. Prioritise measures that can prevent the incident from occurring; in other words, likelihood-reducing measures are to be prioritised above greater emergency preparedness, i.e. consequence-reducing measures.

MATRIX FOR RISK ASSESSMENTS at NTNU

CONSEQUENCE						
	Extremely serious	E1	E2	E3	E4	E5
	Serious	D1	D2	D3	D4	D5
	Moderate	C1	C2	C3	C4	C5
	Minor	B1	B2	B3	B4	B5
	Not significant	A1	A2	A3	A4	A5
		Very low	Low	Medium	High	Very high
		LIKELIHOOD				

Principle for acceptance criteria. Explanation of the colours used in the risk matrix.

Colour		Description
Red		Unacceptable risk. Measures must be taken to reduce the risk.
Yellow		Assessment range. Measures must be considered.
Green		Acceptable risk Measures can be considered based on other considerations.

Appendix A2
Equipments and components

The tables gives an overview of the different components that were used to carry out the experiments at the laboratory.

Instrument	Output signal	Manufacturer	Model
Manometer	mV	DPM	TT470S
Humidity meter	mA	VAISALA	HMT333
Orifice plate	Pa	Lab	
Pitot tube	Pa	Lab	
Thermocouples	mV	Lab	T type
Endoscope	Photo	MEDIT	SCVBS5.5-1
Data logger		National Instruments	NI Cdaq-9178
Air handling unit		Covent	CEAE-035
Solenoid valve	Degree of opening	ASCO	SC E210
Fan		OSTBERG	CK 100A

Description	Manufacturer	Material	Model
Membrane energy exchanger	Lab	Membrane, Aluminum mesh and plastic	Custom made
Air diffusor	Lab		Custom made
Pipe		Aluminum	

Appendix A3
Equipment used in VOC measurements

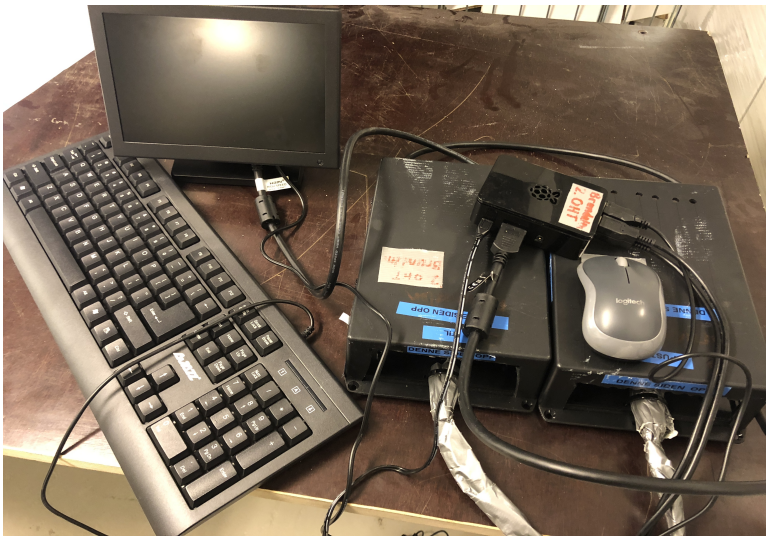

The complete sensor test rig

The figure shows the equipment used to measure the formaldehyde concentrations. The equipment include sensor rigs, a Rasberry Pi computer and a computer screen. Two sensor rigs had to be connected to the Rasberry Pi computer for the computer to create log files.

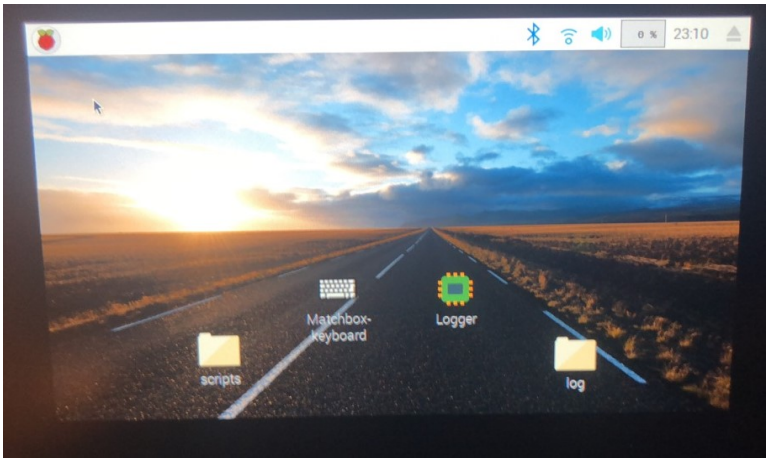

The Rasberry Pi screen

The figure shows the Rasberry Pi desktop. The Logger-file seen in the picture was used to run the script. In the scripts folder, the main script written in c++ could be found, and the log time could be chosen. The log files was found in the log-folder named either TIL or PUST depending on which sensor rig it belonged to.

Appendix A4
Results: Effectiveness measurements

Experimental results at airflow rate 4.30 l/s

The tables below gives more information on the measured data for the lowest airflow rate. This section provides more detailed results for the measurements at airflow rate 4.30 l/s.

Test	T_{SI} [°C]	T_{SO} [°C]	T_{EI} [°C]	T_{EO} [°C]	φ_{SI} [%]	φ_{SO} [%]	φ_{EI} [%]	φ_{EO} [%]	$\dot{V}$ [l/s]	P [Pa]
0.1	14.5	22.3	22.7	15.8	40.7	43.0	44.4	42.8	4.20	255
0.5	6.24	22.0	22.8	8.71	23.0	39.5	42.4	36.8	4.30	254
1.1	-0.32	19.4	20.3	2.84	16.2	31.3	34.4	32.1	4.30	229
2.1	1.47	20.9	22.4	3.71	16.8	36.9	40.2	41.0	4.30	240
3.1	2.76	20.9	21.8	5.42	16.4	45.2	49.4	41.5	4.10	240
4.1	-3.78	20.2	21.8	-0.87	10.2	19.9	21.8	26.0	4.20	244
5.1	-3.73	18.3	19.2	-0.04	11.7	37.3	41.0	37.4	4.30	239
5.2	-4.18	18.6	19.9	-0.94	11.3	39.9	43.7	36.9	4.30	240

Test	ω_{SI} [kg/kg]	ω_{SO} [kg/kg]	ω_{EI} [kg/kg]	ω_{EO} [kg/kg]	ε_S [%]	ε_L [%]	ε_S,ex.side [%]	ε_L,ex. side [%]
0.1	0.0043	0.0074	0.0079	0.0049	95.2	87.8	83.3	82.2
0.5	0.0014	0.0067	0.0076	0.0026	95.2	85.9	85.1	79.9
1.1	0.0006	0.0045	0.0053	0.0015	95.3	83.7	84.7	80.4
2.1	0.0007	0.0059	0.0070	0.0021	93.1	82.0	89.3	78.5
3.1	0.0008	0.0072	0.0083	0.0024	95.5	85.3	86.0	78.9
4.1	0.0003	0.0030	0.0037	0.0009	93.5	80.6	88.6	80.8
5.1	0.0003	0.0050	0.0059	0.0014	96.1	85.1	83.9	80.1
5.2	0.0003	0.0055	0.0065	0.0013	94.8	83.5	86.5	83.6

Experimental results at airflow rate 6.6 l/s

This section provides more detailed results for the measurements at airflow rate 6.60 l/s.

Test	T_{SI} [°C]	T_{SO} [°C]	T_{EI} [°C]	T_{EO} [°C]	φ_{SI} [%]	φ_{SO} [%]	φ_{EI} [%]	φ_{EO} [%]	$\dot{V}$ [l/s]	P [Pa]
0.1	16.1	21.9	22.3	17.2	43.0	33.7	33.6	39.7	6.30	422
0.5	4.12	21.5	22.7	7.17	29.4	38.1	42.6	44.0	6.40	419
1.1	0.43	21.6	23.1	4.17	24.3	24.4	27.4	35.6	6.50	423
1.2	-0.19	19.9	21.7	2.80	23.4	27.3	30.4	39.0	6.60	435
1.3	-0.31	19.8	21.6	2.53	23.7	27.6	31.2	39.5	6.70	445
2.1	-0.04	20.5	22.3	2.95	21.7	34.8	39.1	48.1	6.50	428
3.1	0.13	18.2	19.7	2.79	23.0	37.6	43.4	41.8	6.50	431
4.1	-4.22	20.8	22.2	0.93	16.3	21.2	24.0	32.1	6.80	418
5.1	-4.09	21.3	23.0	0.28	16.1	30.6	34.6	47.9	6.50	418
7.1	-7.80	20.5	22.1	-2.05	14.4	26.9	30.4	42.4	6.60	421
7.2	-7.03	20.4	22.0	-1.71	14.5	27.3	30.9	44.0	6.60	425
8.1	-8.09	20.4	22.1	-2.65	14.4	27.8	31.2	43.4	6.60	426
8.2	-7.94	20.9	23.0	-3.16	13.1	29.1	32.7	44.1	6.60	425
9.1	-6.05	20.3	21.8	-0.73	15.2	42.8	48.4	50.1	6.60	417

Test	ω_{SI} [kg/kg]	ω_{SO} [kg/kg]	ω_{EI} [kg/kg]	ω_{EO} [kg/kg]	ε_S [%]	ε_L [%]	ε_S,ex.side [%]	ε_L,ex. side [%]
0.1	0.0050	0.0057	0.0058	0.0050	93.6	83.0	81.7	104
0.5	0.0015	0.0063	0.0076	0.0028	93.5	78.6	83.6	78.4
1.1	0.0010	0.0040	0.0050	0.0019	93.4	76.5	83.5	77.9
1.2	0.0009	0.0041	0.0051	0.0018	92.0	76.0	86.3	77.2
1.3	0.0009	0.0041	0.0052	0.0018	91.6	74.4	87.0	78.2
2.1	0.0008	0.0054	0.0068	0.0023	92.2	77.1	86.6	75.3
3.1	0.0009	0.0050	0.0064	0.0020	92.5	75.5	86.4	80.3
4.1	0.0005	0.0033	0.0041	0.0013	94.8	78.6	80.5	76.3
5.1	0.0005	0.0050	0.0063	0.0019	93.6	77.7	83.9	75.3
7.1	0.0003	0.0042	0.0052	0.0014	94.7	79.1	80.7	77.4
7.1	0.0003	0.0042	0.0053	0.0015	94.5	78.6	81.7	76.3
8.1	0.0003	0.0043	0.0053	0.0014	94.5	79.0	82.0	78.6
8.2	0.0003	0.0046	0.0059	0.0014	93.1	77.0	84.6	81.0
9.1	0.0004	0.0065	0.0081	0.0018	94.8	79.8	80.8	81.1

Experimental results at airflow rate 8.20 l/s

This section provides more detailed results for the measurements at airflow rate 8.20 l/s.

Test	T_{SI} [°C]	T_{SO} [°C]	T_{EI} [°C]	T_{EO} [°C]	φ_{SI} [%]	φ_{SO} [%]	φ_{EI} [%]	φ_{EO} [%]	$\dot{V}$ [l/s]	P [Pa]
0.1	19.9	22.9	23.3	20.4	44.5	45.7	47.7	47.3	7.90	556
0.2	16.1	22.5	23.0	17.5	48.5	43.2	45.0	48.4	8.00	567
0.3	14.9	21.8	22.3	16.4	48.2	43.4	45.3	48.5	8.00	566
0.5	4.44	21.4	22.7	7.99	34.0	36.0	40.5	46.9	8.10	563
1.1	-1.30	20.0	21.6	3.15	21.2	21.2	24.5	32.0	8.20	565
1.2	-0.55	21.4	23.0	4.18	26.0	24.4	27.9	39.2	8.20	557
2.1	0.18	18.6	20.1	3.15	25.8	34.7	40.0	42.4	8.20	-
3.1	-1.42	19.4	21.2	2.45	21.0	43.0	49.8	53.4	8.20	556
4.1	-4.24	18.6	21.5	-1.04	20.8	19.0	21.8	33.8	8.20	558
5.1	-4.56	18.1	19.2	0.74	19.1	33.7	39.7	44.3	8.20	552
6.1	-4.41	20.7	22.8	0.25	19.8	44.5	50.7	55.4	8.20	562
7.1	-8.83	18.7	21.2	-3.70	17.8	22.6	26.1	41.3	8.30	561
7.2	-9.15	19.3	21.4	-3.27	17.6	25.2	28.7	42.6	8.30	571
7.3	-10.5	18.8	21.7	-5.75	15.1	24.0	27.4	41.4	8.20	566
9.1	-6.87	20.0	21.6	-1.19	16.1	42.0	48.1	46.4	7.80	543

Test	ω_{SI} [kg/kg]	ω_{SO} [kg/kg]	ω_{EI} [kg/kg]	ω_{EO} [kg/kg]	ε_S [%]	ε_L [%]	ε_S,ex.side [%]	ε_L,ex. side [%]
0.1	0.0066	0.0082	0.0088	0.0073	88.1	73.8	85.4	70.5
0.2	0.0057	0.0076	0.0081	0.0062	92.4	76.9	80.2	78.9
0.3	0.0052	0.0073	0.0079	0.0058	92.8	77.9	79.8	78.4
0.5	0.0018	0.0059	0.0072	0.0032	93.2	76.3	80.5	74.2
1.1	0.0007	0.0032	0.0041	0.0016	92.9	73.3	80.6	75.8
1.2	0.0010	0.0040	0.0050	0.0020	93.3	74.5	79.9	73.4
2.1	0.0010	0.0047	0.0060	0.0021	92.3	74.4	85.1	79.2
3.1	0.0007	0.0062	0.0081	0.0025	92.1	74.9	82.9	76.4
4.1	0.0006	0.0026	0.0036	0.0012	88.6	67.2	87.6	79.2
5.1	0.0005	0.0045	0.0057	0.0018	95.2	76.7	77.7	75.1
6.1	0.0006	0.0070	0.0091	0.0022	92.3	75.4	82.9	80.9
7.1	0.0004	0.0031	0.0042	0.0012	91.6	71.6	82.9	77.7
7.2	0.0003	0.0036	0.0047	0.0013	92.9	74.4	80.8	78.2
7.3	0.0003	0.0033	0.0046	0.0010	91.1	71.4	85.3	81.8
9.1	0.0004	0.0063	0.0080	0.0016	94.3	77.6	80.0	83.3

Appendix A5

Results: Formaldehyde measurements

Test 0

Test 0 consist of initial measurements to evaluate the surrounding environment. Figure 8.1 and 8.2 shows the formaldehyde concentrations in the laboratory room and in the cold chamber during work hours. The time stamp in figure 8.1 is wrong, and in reality it should be the same as in figure 8.2. This is due to some problems with changing the time on the Rasberry Pi computer, but the time stamps on the other figures in the further testing are correct.

The MEE was in working mode during the measurements in figure 8.1 and 8.2 according to the operating conditions mentioned in the chapter about experimental method. The formaldehyde concentrations during work hours could get quite high in the laboratory room, as shown in figure 8.1. The following experiments were then executed outside of ordinary work hours to have better control over the concentration from outside sources.

Figure 8.1: The formaldehyde concentration in the laboratory during work hours

Figure 8.2 shows the ”outside” concentration. Two sensors were placed in the cold chamber next to the supply inlet duct since the Rasberry Pi needs two sensors to be able to log. The sensor marked ”PUST” was placed on the wall next to the duct, while the sensor marked ”TIL” was placed below the duct.

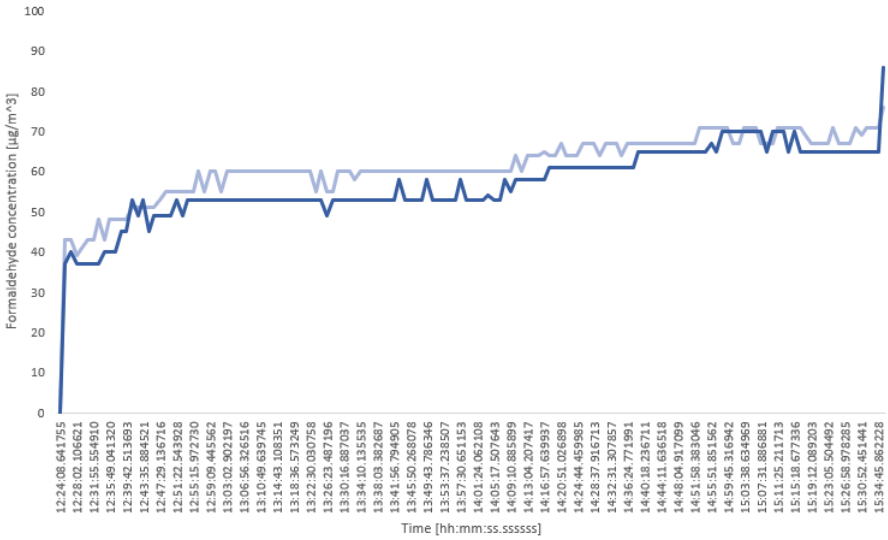

Figure 8.2: The formaldehyde concentration in the cold chamber during work hours

Figure 8.3 shows the formaldehyde concentrations measured by the sensors during a 24-hour period in the weekend, and the MEE was turned off during this period. There are some variations in the concentrations during the course of this day, especially for the supply-outlet measurements. There is also clearly some formaldehyde source in the cold chamber as the concentration gradually increases during the day. However, these concentrations are much more stable than the ones measured during work hours, so the following tests were performed outside of ordinary working hours.

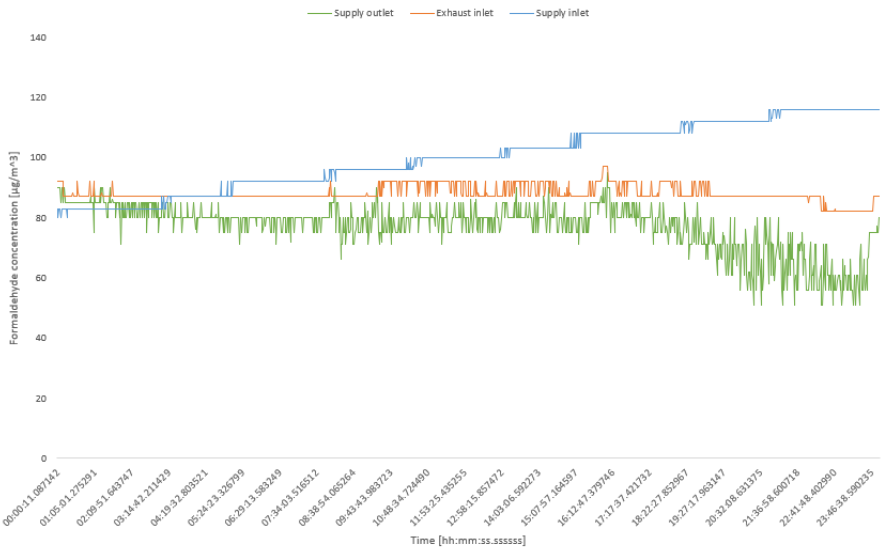

Figure 8.3: Formaldehyde concentrations in the lab during a 24-hour period in the weekend

Results from formaldehyde test 1-6

The following sections presents the results from the formaldehyde measurements in more detail. The values for temperature and relative humidity in the tables are the average of the logged values during the time the particleboard were placed in the AHU. Likewise, the effectiveness values are the average values for the same period. The pressure over the orifice plate was kept constant during the measurements, and the resulting air flow rate was calculated by the same method as stated in chapter 4. As for the pressure drop, the value is the mean of the pressure drops given by the manometers.

The formaldehyde concentrations presented in the tables are the average concentrations measured by each of the sensors before and after the particleboard was placed by the exhaust inlet duct. The EATR value is the average exhaust air transfer rate for the time period with the particleboard.

Each of the graphs in the following sections show how the concentration measured by the sensors changes with time. The chosen time step was 75 s, and the particleboard was placed at the exhaust inlet 30 min after the start of the graph. It is worth noting that the MEE had been running for a while before this, so the MEE conditions were stable from the start of the graphs.

Measurement number 1

The operating conditions and the results for test number 1

	Supply inlet	Supply outlet	Exhaust inlet
T [$^{\circ}$C]	14.5	22.3	22.7
ϕ [%]	40.7	43.0	44.4
$\bar{C}_{HCHO,before}$ [$\mu g/m^3$]	106	144	114
$\bar{C}_{HCHO,after}$ [$\mu g/m^3$]	108	174	227
$\dot{V}$ [l/s]		4.2	
P [Pa]		255	
ε_S[%]		95.22	
ε_L[%]		87.8	
EATR [%]		55.0	

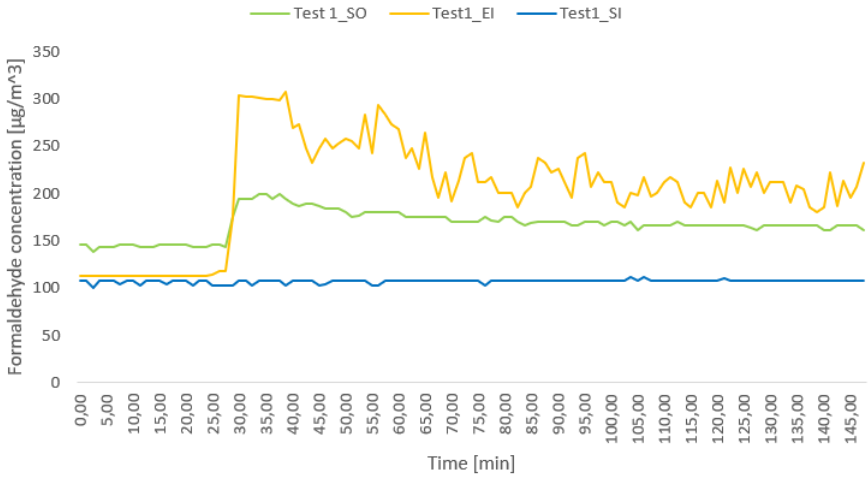

The formaldehyde concentrations measured by each of the sensors in test 1

Measurement number 2

The operating conditions and the results for test number 2

	Supply inlet	Supply outlet	Exhaust inlet
T [°C]	16.1	21.9	22.3
ϕ [%]	43.0	33.6	33.6
$\bar{C}_{HCHO,before}$ [$\mu g/m^3$]	121	124	87.0
$\bar{C}_{HCHO,after}$ [$\mu g/m^3$]	123	148	207
$\dot{V}$ [l/s]		6.3	
P [Pa]		422	
ε_S[%]		93.6	
ε_L[%]		83.0	
EATR [%]		29.3	

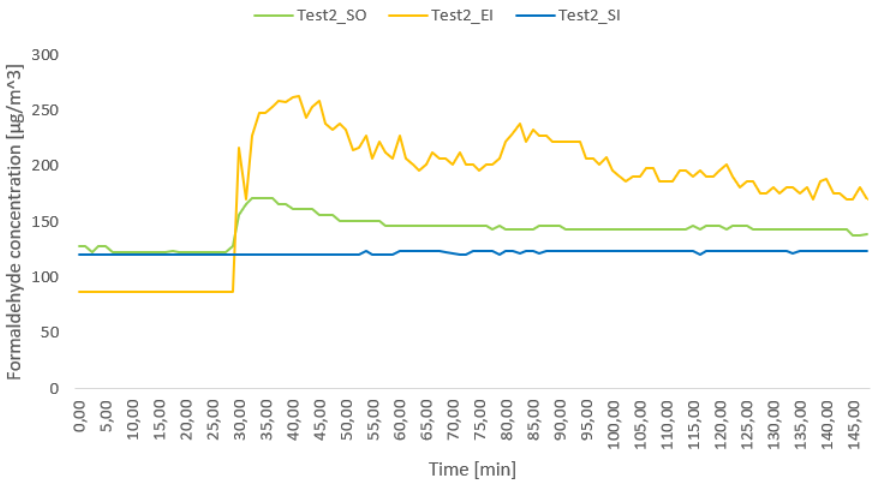

The formaldehyde concentrations measured by each of the sensors for test 2

Measurement number 3

The operating conditions and the results for test number 3

	Supply inlet	Supply outlet	Exhaust inlet
T [$^{\circ}$C]	14.9	21.8	22.3
ϕ [%]	48.2	43.4	45.4
$\bar{C}_{HCHO,before}$ [$\mu g/m^3$]	125	160	134
$\bar{C}_{HCHO,after}$ [$\mu g/m^3$]	132	184	234
$\dot{V}$ [l/s]		8.0	
P [Pa]		566	
ε_S[%]		92.8	
ε_L[%]		77.9	
EATR [%]		51.1	

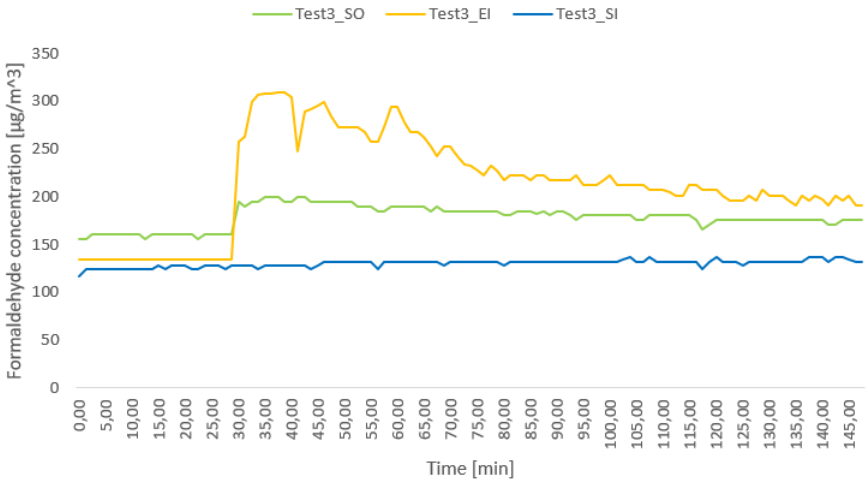

The formaldehyde concentrations measured by each of the sensors for test 3

Measurement number 4

The operating conditions and the results for test number 4

	Supply inlet	Supply outlet	Exhaust inlet
T [$^{\circ}$C]	6.24	22.0	22.8
ϕ [%]	23.0	39.5	42.4
$\bar{C}_{HCHO,before}$ [$\mu g/m^3$]	24.0	85.2	78.5
$\bar{C}_{HCHO,after}$ [$\mu g/m^3$]	22.2	125	226
$\dot{V}$ [l/s]		4.3	
P [Pa]		254	
ε_S[%]		95.2	
ε_L[%]		85.9	
EATR [%]		50.5	

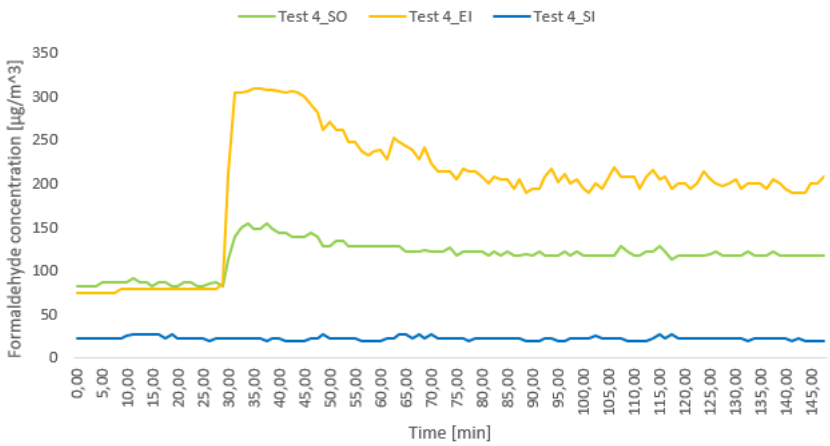

The formaldehyde concentrations measured by each of the sensors for test 4

Measurement number 5

The operating conditions and the results for test number 5

	Supply inlet	Supply outlet	Exhaust inlet
T [$^{\circ}$C]	4.12	21.5	22.7
ϕ [%]	29.4	38.1	42.6
$\bar{C}_{HCHO,before}$ [$\mu g/m^3$]	24.7	89.3	86.1
$\bar{C}_{HCHO,after}$ [$\mu g/m^3$]	27.1	113	204
$\dot{V}$ [l/s]		6.4	
P [Pa]		419	
ε_S[%]		93.5	
ε_L[%]		78.6	
EATR [%]		48.3	

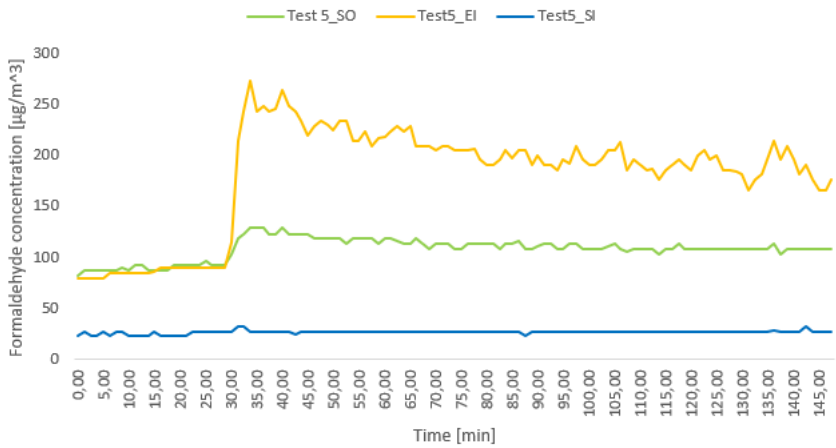

The formaldehyde concentrations measured by each of the sensors for test 5

Measurement number 6

The operating conditions and the results for test number 6

	Supply inlet	Supply outlet	Exhaust inlet
T [$^{\circ}$C]	4.44	21.4	22.7
ϕ [%]	34.0	36.0	46.9
$\bar{C}_{HCHO,before}$ [$\mu g/m^3$]	40.9	81.9	78.3
$\bar{C}_{HCHO,after}$ [$\mu g/m^3$]	37.8	107	170
$\dot{V}$ [l/s]		8.1	
P [Pa]		563	
ε_S[%]		93.2	
ε_L[%]		76.3	
EATR [%]		52.1	

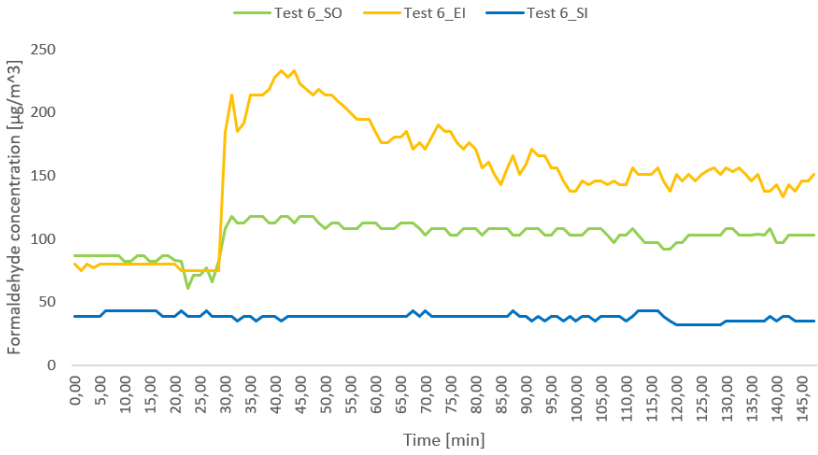

The formaldehyde concentrations measured by each of the sensors for test 6

Repeat of measurement 2

The operating conditions and the results for test number 2.2

	Supply inlet	Supply outlet	Exhaust inlet
T [$^{\circ}$C]	15.1	21.9	22.4
ϕ [%]	56.7	40.3	39.5
$\bar{C}_{HCHO,before}$ [$\mu g/m^3$]	75.3	96.6	82.0
$\bar{C}_{HCHO,after}$ [$\mu g/m^3$]	94.7	132	186
$\dot{V}$ [l/s]		6.3	
P [Pa]		415	
ε_S[%]		93.4	
ε_L[%]		89.7	
EATR [%]		41.0	

The formaldehyde concentrations measured by each of the sensors for test 2.2

Repeat of measurement 3

The operating conditions and the results for test number 3.2

	Supply inlet	Supply outlet	Exhaust inlet
T [$^{\circ}$C]	16.1	22.5	23.0
ϕ [%]	48.5	43.2	45.0
$\bar{C}_{HCHO,before}$ [$\mu g/m^3$]	144	183	123
$\bar{C}_{HCHO,after}$ [$\mu g/m^3$]	144	191	194
$\dot{V}$ [l/s]		8.00	
P [Pa]		567	
ε_S[%]		92.4	
ε_L[%]		76.9	
EATR [%]		93.8	

The formaldehyde concentrations measured by each of the sensors for test 3.2

Maren Evensen

Membrane Energy Exchanger

NTNU
Norwegian University of
Science and Technology